Cold Spray Deposition of Titanium onto Aluminium Substrates

Maria Manuel Fernandes Barbosa

Porto, Julho de 2009

Tese de Mestrado orientada por:

Professor Fernando Jorge Monteiro, Faculdade de Engenharia, Universidade do Porto

Professor Josep Maria Guilemany, Centro de Projecção Térmica, Universidade de Barcelona

Dissertação submetida à Universidade do Porto para a obtenção do grau de Mestre em Engenharia Metalúrgica e de Materiais.

CANDIDATO	Maria Manuel Fernandes Barbosa		**CÓDIGO:** 050508013
TÍTULO	Cold Spray Deposition of Titanium onto Aluminium Substrates		
DATA	23 de Julho de 2009		
LOCAL	Faculdade de Engenharia da Universidade do Porto – Sala B033, 16h00		
JÚRI	Presidente	Professor Doutor Luís Filipe Malheiros, DEMM/FEUP	
	Arguente	Professor Doutor Rui Silva, DECV/UA	
	Orientador	Professor Doutor Josep Maria Guilemany, DCMM/UB	
	Orientador	Professor Doutor Fernando Jorge Monteiro, DEMM/FEUP	

"Posso ter defeitos, viver ansioso e ficar irritado algumas vezes
mas não esqueço que a minha vida é a maior empresa do mundo.
E que posso evitar que ela vá à falência.
Ser feliz é reconhecer que vale a pena viver, apesar de todos os desafios.
Ser feliz é deixar de ser vítima dos problemas e tornar-se autor da própria história.
É atravessar desertos fora de si, mas ser capaz de encontrar um oásis no recôndito da alma.
É agradecer a Deus a cada manhã pelo milagre da vida.
Ser feliz é não ter medo dos próprios sentimentos.
É saber falar de si mesmo. É ter coragem para ouvir um "não".
É ter segurança para receber uma crítica, mesmo que injusta.
Pedras no caminho? Guardo-as todas, um dia vou construir um castelo... "

Fernando Pessoa

Dedico esta memória aos meus pais,
sem os quais nada seria possível!

Agradecimentos

Nao há trabalhos difíceis quando estamos rodeados de pessoas que amam o que fazem e que nos contagiam com o seu espirito. Eu tive a sorte de cruzar o meu caminho com algumas delas!

Moltes gràcies al Professor Guilemany per donar-me l'oportunitat de treballar en el seu grup, confiar sempre en mi i, per la paciència que ha demostrat en tot moment a l'hora de fer de tutor (i amic) durant aquests mesos. A Núria Cinca per estar sempre disposada a donar-me el seu suport i dedicar-me el seu temps, per compartir els seus coneixements amb mi, ser la millor companya de treball i, sobretot, també una bona amiga. A Sergi Dosta, per haver-me ajudat a l'obtenció dels recobriments gràcies a la seva experiència en Projecció Tèrmica i per les llargues discussions sobre els paràmetres òptims del procés, però també pel seu bon humor en tot moment.

No vull oblidar-me de la companyia, simpatia i valorable ajuda de la resta de membres del grup, començant pel Dr. Joan Ramón Miquel, el Prof. Javier Fernández, la Dra. Irene Garcia Cano i seguint pels companys i amics del dia a dia com la Sandra, Jèssica, María, Vero, Judith, Esther i Víctor.

Muito obrigada ao Professor Luís Filipe Malheiros por todo o acompanhamento durante os meus 4 anos de Engenharia Metalúrgica e por possibilitar este pequeno grande estágio no CPT. Ao Professor Fernando Jorge Monteiro por ter tanta pacienciência para mim e por ser um dos melhores orientadores, nao só na vida académica mas também quando preciso de um amigo. Ao Professor Manuel Vieira e à Professora Filomena Viana, apesar de não tão próximos neste último ano, serem quem mais aturou as minhas loucuras e partilhou os meus momentos. E claro, a minha vida na FEUP nao seria a mesma sem o Paulinho, a Cátia e o Rúben, meus eternos companheiros.

Também ao Manel, à Lili e ao André, melhores amigos de quem tive tantas saudades em Barcelona. E ao Marcus, à Stina, ao Oliver e ao Nathan por preencherem o meu espaço, me fizeram sentir em casa e serem os melhores amigos que podia encontrar.

E por último, mas mais importante, aos meus pais e ao meu irmão, que sempre me ajudaram a realizar os meus sonhos e a conquistar os meus medos, e sem os quais nao seria quem sou nem chegaria onde estou e aonde ainda sonho chegar!

Muito Obrigada!

Abstract

The aluminium alloy 7075-T6 is widely used in aeronautic engineering due to its high mechanical resistance to weight ratio. Depending upon the environmental conditions, many types of corrosion mechanisms have been found to occur in aircraft structural aluminium alloys. A possible solution to improve the alloy's behaviour is the deposition of a pure Titanium coating. At present the deposition of Titanium is limited to processes such as Electroplating, Chemical Vapour Deposition and Vacuum Plasma Spray. These traditional approaches are generally slow and expensive, while the common thermal spray processes have two major limitations which are the presence of porosity and oxides in the spray-deposited material. Since Titanium is a metal very sensitive to oxidation, it is proposed in the present work to deposit it onto Aluminium substrates by a novel thermal spray process known as "Cold Spray". In this work, the influence of the gas pressure and temperature, and the powder feeding rate on the cold spray process and in the final coating characteristics was studied, and a dense pure titanium coating onto aluminium 7075 substrates, with thickness higher than 300μm and no microstructural changes was easily and fast obtained. It was possible to conclude that after optimization, the cold spray process when compared to the conventional thermal spray techniques, results in coatings with very good properties and cost-time effective (higher coating thickness can be achieved in less time and with less money investment), making it ideal for industrial applications.

Contents

1. Importance of Aluminium and Alloys

Aluminium, the second most abundant metallic element on earth, became an economic competitor in engineering applications as recently as by end of the 19th century. The main properties that make aluminium a valuable material are its low density, high strength, corrosion resistance, durability, ductility, formability, conductivity and the possibility to be 100% recycled. Due to this unique combination of properties, the variety of applications of aluminium continues to increase (Figure 1). It is essential in our daily lives. We cannot fly, use a high speed train or a high performance car without it. Nor can we get heat and light into our homes and offices without it. We depend on it to preserve our food, our medicines and to provide electronic components for our computers [1, 2].

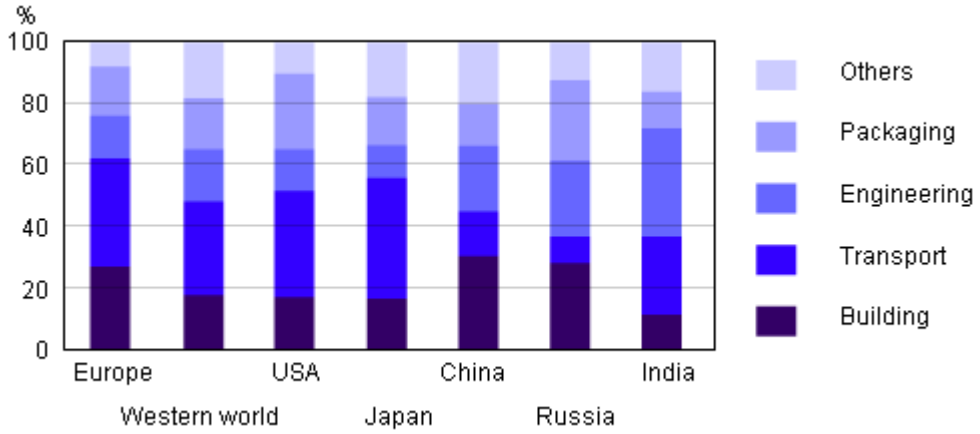

Figure 1 - Different sectors of aluminium applications [1].

For many years the biggest end-use market for aluminium has been the transport sector. The transport industry plays an important role in the European Union economy. It accounts for 7% of Gross National Product, 7% of jobs, 40% of investments by member states and 30% of energy consumption [1, 2]. Aluminium use allows, through its contribution to vehicle lightweighting, substantial energy savings and reduced emission and fuel consumption levels in today's environmentally conscious society (for example the Green Car European Project). Its strength and corrosion-resistance guarantee durability, reliability and security, coupled with cost-effectiveness. Its formability ensures complete flexibility of design and ease of handling. Finally, its total recyclability allows the aluminium industry to fulfil its commitment to the principles of sustainable development. Today, aluminium is

widely used in cars, trucks, buses, coaches, trains, metros, ships, ferries, aircraft and bicycles.

There are two main classes of aluminium alloys: wrought and cast alloys. The first ones are initially casted as ingots or billets and subsequently hot and/or cold worked mechanically into the desired shape. The alloys of the second type are directly cast into their final form by one of various methods such as sand-casting, die or pressure die casting. These two main classes of alloys have different classification systems. It will be shortly explained the nomenclature of the wrought aluminium alloys since it is this group that includes the material used as substrate in this work.

The 8 series of wrought alloys are designated by a 4 digit number that may be preceded or followed by letters. A prefix is used to designate the standard AA of the Aluminium Association or EN AW for the European standard. The first digit indicates the series as shown in Figure 2. The second digit indicates alloy modifications of an already existing alloy, and the third and fourth may have different meanings depending on the first one. For the series 2xxx to 8xxx, the 3rd and 4th digits identify a specific alloy without physical significance.

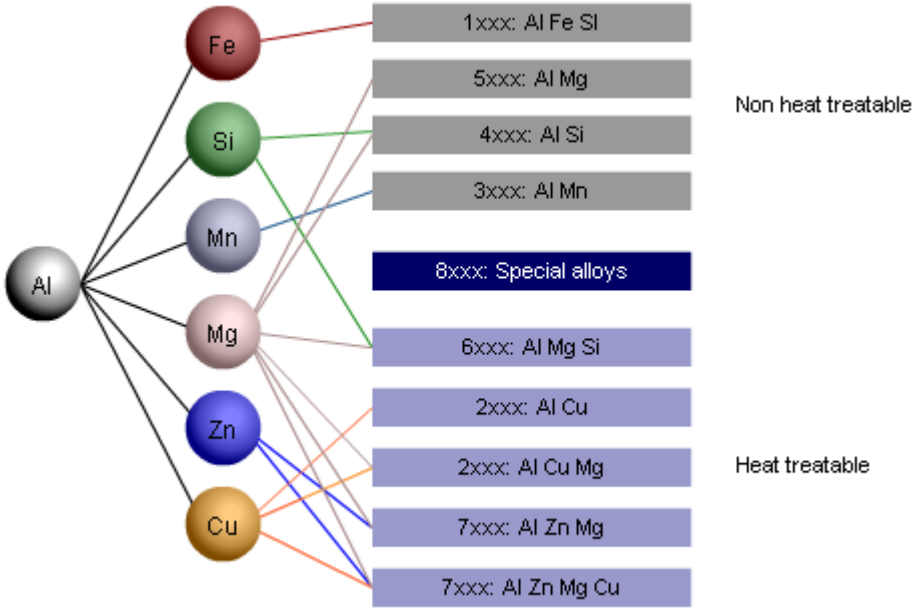

Figure 2 - Wrought aluminium alloy nomenclature system [1].

The alloy used in this work, 7075-T6, belongs to the 7xxx series. In general they are very strong "heat treatable" alloys, since they can be strengthened through heat treatment

(precipitation hardening) based on the combination of zinc (mostly between 4–6 wt %) and magnesium (range 1–3 wt %). Unfortunately these alloys seem prone to stress cracking. As with some of the 2xxx series, alloys in the 7xxx series also have additions of magnesium to maximise their age-hardening potential where the precipitating phases are typically of the type $MgZn_2$. Such alloys give medium strength, but are relatively easily welded. Aluminium-zinc-magnesium alloys have a greater response to heat treatment than the binary aluminium-zinc alloys resulting in higher strengths. The additions of zinc and magnesium however decrease the corrosion resistance. Chromium amounts, generally less than 0.35 %, are added to increase the electrical resistivity and to control grain structure, by preventing re-crystallisation in aluminium-magnesium-silicon and aluminium-zinc alloys during hot-working or heat-treatment. The addition of copper to aluminium-zinc-magnesium alloys, together with small amounts of chromium and manganese, results in the highest strength aluminium alloys available. Alloys based on the quaternary Al–Zn–Mg–Cu system have the greatest potential of all aluminium alloys for age-hardening, and yield strengths approaching 600 MPa can be achieved in some alloys. Zinc and magnesium control the ageing process, while the effect of copper is the increase in ageing rate and the increase in quench sensitivity. Although copper decreases the general corrosion resistance, it improves the resistance to stress cracking [1, 2]. For a more thorough analysis of the 7075-T6 properties please check Annex 1 [1].

T6 is the designation to the solution heat-treated and artificially aged alloys. It represents a group of products that are not cold-worked after solution heat-treatment and for which mechanical properties or dimensional stability, or both, have been substantially improved by precipitation heat-treatment [2].

Important critical applications of the 7075-T6 alloy are based on its superior strength, for example in aerospace, space exploration, military and nuclear applications. But also structural parts in building applications, as well as high strength sports' attributes such as ski poles and tennis rackets.

2. Titanium Coating

By nature, aluminium is a highly reactive material. Fortunately it rapidly forms a thin and dense oxide layer that protects the underlying material, and that if damaged, re-forms immediately in most environments. The presence of this oxide layer makes aluminium very suitable for many applications.

Although the addition of alloying elements may increase significantly the mechanical properties in the 7075-T6 alloy, the high corrosion resistance characteristic of most aluminium alloys is seriously affected. The decrease in corrosion resistance with increasing copper content is not primarily attributable to these solid-solution or second phase solution-potential relationships, but to galvanic cells created by formation of minute copper particles or films deposited on the alloy surface as a result of corrosion [1].

Nevertheless, this alloy seeks heavy duty use in the aircraft industry where the environment is typically mild and aluminium corrosion isn't likely to occur. Although, if we want to aim higher and be able to use this alloy under more specific conditions, like for example in the structure of a satellite, or a rocket, that will have to cross the atmosphere barrier, resistance to corrosion will be required.

A possible approach to increase the corrosion resistance of this alloy is the deposition of a pure titanium coated layer. Titanium is now being viewed, accepted and used as a material for the prevention of corrosion, the reduction and elimination of major corrosion related maintenance issues and for the advantages that it offers in weight savings, replacement costs and life cycle cost benefits. And if we oxidize the titanium coating into TiO2, with a laser, we will have a coating that will withstand high temperature and wear.

Titanium is lightweight, has high tensile strength, has the ability to withstand moderately high temperatures without creeping, is corrosion resistant and is abundant in nature. Titanium and its alloys possess tensile strengths from 210 to 1380 MPa, which are equivalent to the strengths found in most of alloy steels. The density of titanium is only 56 percent that of steel and its corrosion resistance compares well with that of platinum. Due to these properties titanium is commonly used in aircraft, pipes for power plants, armour plating, naval ships, spacecraft and missiles [2, 3]. For a thorougher analysis of commercially pure titanium properties please check Annex 2 [2].

2.1 Titanium's deposition techniques

At present the cost-efficient deposition of Titanium is limited to processes such as Electroplating, Low-Pressure Chemical-Vapour Deposition and Vacuum Plasma Spray techniques that manage to limit the contact of Titanium with Oxygen and avoid unwanted phases.

The electroplating procedure involves electrolysis of potassium titanium fluoride dissolved in alkali or alkaline earth halides under an inert atmosphere. Graphite or titanium metal anodes are employed. It allows the production of adherent titanium coatings up to 100μm thick. Coatings are essentially pure titanium and underneath the coating there is a substrate metal-titanium alloy layer producing a firm metal-metal bonding [4]. It is a very slow process that requires well adjusted parameters and a special attention to the reaction products since it might be not-environmental-friendly.

Other alternative is chemical vapour deposition (CVD) which involves the formation of a thin solid film on a substrate material by a chemical reaction of vapour-phase precursors [5]. The chemical reactions of precursor species occur both in the gas phase and on the substrate. A more detailed picture of the basic physicochemical steps in an overall CVD reaction is illustrated in Figure 3, which indicates several key steps. First the evaporation and transport of reagents (i.e. precursors) in the bulk gas flow region into the reactor; Second, the gas phase reactions of precursors in the reaction zone to produce reactive intermediates and gaseous by-products; Next, mass transport of reactants to the substrate surface and adsorption of the reactants on the substrate surface, followed by surface diffusion to growth sites, nucleation and surface chemical reactions leading to film formation. Finally, there is desorption and mass transport of the remaining fragments of the decomposition away from the reaction zone.

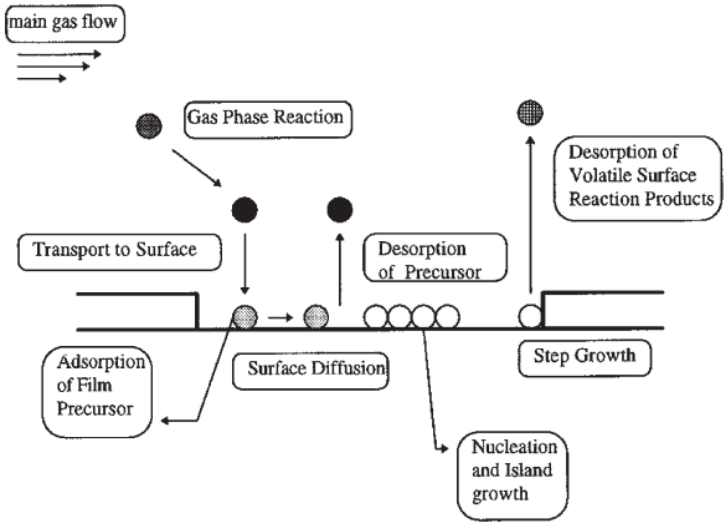

Figure 3 – Precursor transport and reaction processes in CVD [7].

Titanium is deposited by Low-Pressure CVD, which is a CVD processes at sub-atmospheric pressures. The reduced pressures tend to reduce unwanted gas-phase reactions and

improve film uniformity across the substrate. Equation 1 represents the typical reaction to obtain a pure titanium film through this method for semiconductor devices [6]:

$$TiCl_4 + 2H_2 \rightarrow Ti + 4HCl \quad (1)$$

CVD is most versatile at temperatures over 600°C, so its application is limited to substrates that are stable at such temperatures, which isn't the case of the aluminium alloy 7075-T6 since its melting temperature its between 477-635°C. A second problem is that some chemical precursors are hazardous or extremely toxic, requiring closed system and makes it not-environmental-friendly. Finally, the efficiency of the process is sometimes low, resulting in high costs.

The other option, Plasma spray (Figure 4) is a widely used electrical thermal spray process. The conventional process is commonly referred to as air or atmospheric plasma spray (APS). In this process, "plasma" based on a partially ionized conductive gas, is used to melt and propel powdered feedstock material onto the substrate. To create the plasma jet, inert plasma-forming gas, usually argon or nitrogen with minor additions of helium or hydrogen, is injected into the annular space between two cylindrical electrodes, and a high and DC current arc is then struck between the electrodes [7]. The arc partially ionizes the gas and the collisions between energised ions forms a high-temperature, electrically conductive plasma, which expands and escapes through the open end of the anode to form a very hot, high-velocity, plasma jet. The exit velocity will depend on the design of the anode (nozzle) and the operating conditions, and may be either subsonic or supersonic. Powder feedstock is introduced via an inert carrier gas and is accelerated toward the workpiece by the plasma jet. The plasma temperatures in the powder heating region range from about 6000 to 15000°C, significantly above the melting point of any known material [8]. For this reason, this process is one of the most versatile of all thermal spray processes, able to deposit an exceptionally wide range of materials including metals, many ceramics, glasses, some polymers and unique composite materials. An important variant of plasma spraying can be seen in Figure 5 and is known as vacuum plasma spray (VPS) or low-pressure plasma spray (LPPS). Both refer to plasma spray deposition carried out inside a vacuum chamber at relatively low dynamic pressure of inert gas. The low pressure turns the plasma "flame" wider and longer, through the use of a convergent/divergent nozzle, allows higher speed. The relative absence of oxygen and the ability to operate with higher substrate temperatures produce denser, more adherent coatings with much lower oxide

contents [8]. But current vacuum plasma techniques have one disadvantage: “Anyone using these coatings techniques will be faced to some extent with high investment costs,” says Marko Eichler, a researcher at the Fraunhofer Institut for Thin Films and Surface Engineering IST in Braunschweig. Expensive vacuum pumps and chambers of considerable dimensions are required to generate and maintain the low-pressure environment required for plasma treatment of workpieces [9].

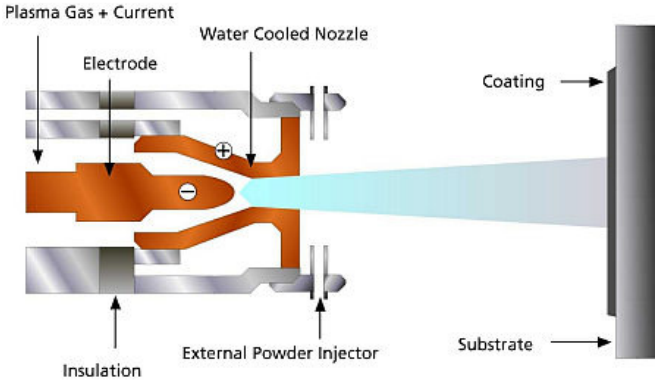

Figure 4 - Schematic diagram of the atmospheric plasma spray process [10].

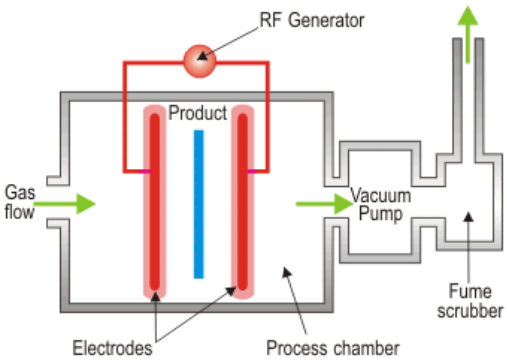

Figure 5 - Schematic of a typical vacuum plasma system [10].

Analyzing the available techniques for titanium deposition and considering our titanium/aluminium system, it is necessary to find an alternative that might allow high deposition rates and high coating quality at relatively low-cost values. Since cold-spray is a 100% solid-state process, the deposition “in air” of titanium coatings without significant oxidation represents an important technical achievement [11], that can potentially allow the deposition of pure titanium onto aluminium substrates at industrial competitive rates and prices.

3. Conventional Thermal Spray techniques

Before entering the cold spray domain, it is important to have a reasonable knowledge of the traditional thermal spray techniques and their advantages and limitations, which will allow a better understanding of the many new possibilities arising from the Cold Spray process.

The term “thermal spray” refers to a broad family of spray process technologies, such as arc spray, plasma spray, flame spray, and high velocity oxy-fuel (HVOF) [8]. And, according to Schoop [13], the group may be large and the specific details different for each

technique, but the fundamental principles for all traditional spray processes are essentially the same.

In a generic thermal spray process (Figure 6), electrical or chemical energy is used to create small molten or semi-molten droplets (typically 10-100 microns in diameter) from powder, wire, or rod feedstock. These droplets are projected onto a workpiece surface by a subsonic or supersonic gas stream at velocities that range from a few tens of meters per second, up to roughly 1000 m/s [7, 13, 14]. Upon impact, each droplet spreads out and quickly solidifies (the cooling time is in the order of nanoseconds), forming the basic microstructural unit of spray-deposited material, called a "splat". Splats randomly stack up on each other forming the layered or lamellar microstructure that is characteristic of most thermal spray deposited materials [7, 14]. The quality of the "splat boundaries", name given to the interface between the solidified particles, strongly influences the physical and mechanical properties of the coating, much like grain boundaries influence the properties of bulk materials.

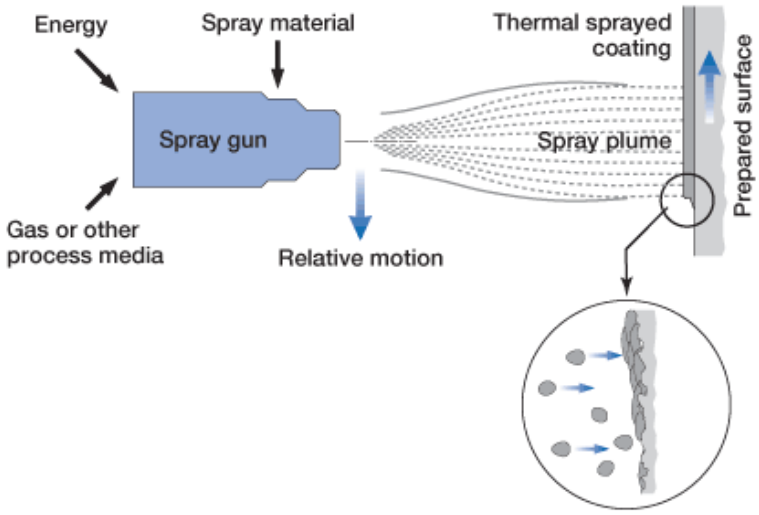

Figure 6 - Generic thermal spray process [13].

The commercially important thermal spray processes can be divided into two basic categories: the ones that use electric energy and the ones that use chemical energy.

Electrical processes typically use either an electric arc or electrically driven plasma to heat and melt the spray material. In the wire arc process (Figure 7) two consumable wire electrodes connected to a high-current direct-current (DC) power source are fed into the gun and meet, establishing an arc between them that melts the tips of the wires [7]. A jet of compressed air or inert gas is directed across the wire tips, atomizing the molten metal

and creating a spray stream of molten droplets. As the tip melt, additional wire is fed into the arc, making this a continuous process. An obvious limitation of this process is that it can only be used to deposit materials that can be made into conductive metal wires. Yet, its simplicity and economy result in a wide range of applications such as spraying zinc- or aluminium-based anti corrosion coatings onto bridges, ship decks, large metal tanks, etc [7, 8]. Another widely used thermal spray process is the APS, which has already been described in the previous section.

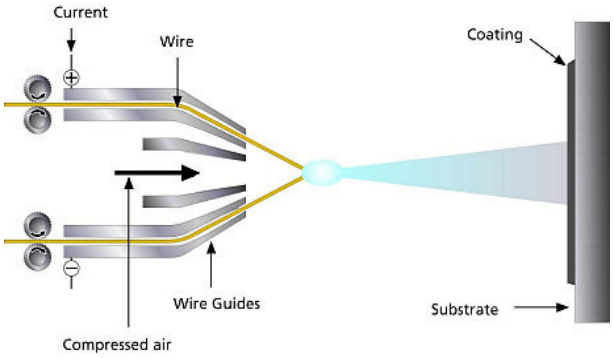

Figure 7 - Schematic diagram of the electric arc thermal spray process [10].

Regarding the chemical energy thermal spray processes, flame spray is an oxy-fuel process that is widely used in industry. It includes low-velocity powder flame, rod flame, and wire flame processes and high-velocity processes such as high-velocity oxy-fuel (HVOF) and the detonation gun (D-gun) process [8]. Burning oxygen with various fuel gases – such as acetylene, propane, or propylene - can produce flame temperatures sufficient to melt many metals and polymers as well as some ceramics. Different flame spray devices are designed to powder, wire, or ceramic rod feedstock. Figure 8 shows a typical flame spray device where a jet of compressed air is used to accelerate the molten droplets toward the substrate. The velocity can range from 50 to 300 m/s depending upon the device's design, the material being sprayed, and the operating conditions. Operations in the lower velocity range tend to produce coatings that are more porous (less dense) than those produced by more energetic spray conditions with higher impact velocities [7]. Due to the reaction with oxygen in the flame and in the air atmosphere, it's frequent that metal deposits have very high oxide content. Nevertheless, the properties of flame-sprayed coatings are well suited for many applications, which, together with its relatively low process cost, make this a favourite process for many commercial purposes.

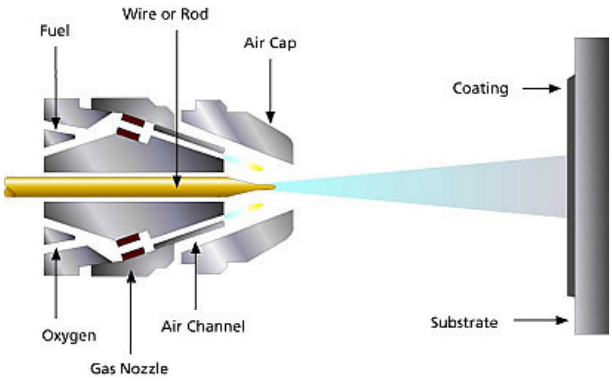

Figure 8 - Schematic diagram of the flame spray process [10].

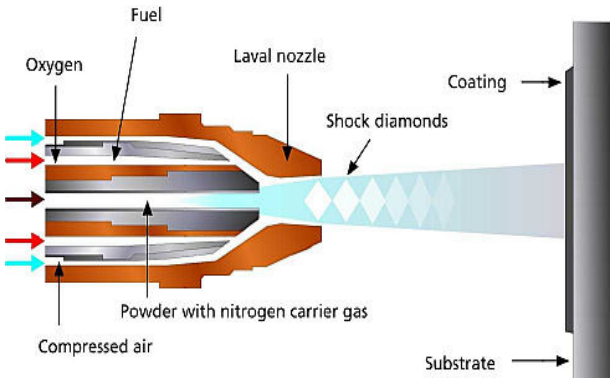

Figure 9 – Schematic diagram of a high-velocity oxy-fuel (HVOF) spray gun [10].

The HVOF process is similar to flame spray in what concerns a fuel gas or liquid fuel that is first mixed with oxygen and then burned in the combustion chamber of the torch (Figure 9). However, in this case, it's a supersonic jet that exits the nozzle, due to the combustion occurring at much higher pressures and to the use of a converging-diverging nozzle. Powder particles entrained in this high-velocity gas jet are accelerated up to velocities of the order of 450-1000 m/s, once again depending upon the spray device, the spray material, and operating conditions [7]. The "peening" effect of these high-velocity particles impacting the surface can produce coatings with very little porosity and also create a more favourable residual compressive stress state in the deposited material. These combinations of properties make HVOF a preferred process for applications such as spraying cemented carbide wear-resistant coatings. The Detonation Gun™ is a process similar in concept to HVOF, but in the case of the D-Gun™ the process is not a continuous combustion. Here, pre-encapsulated "shots" of feedstock powder are fed into a 1m long barrel along with oxygen and a fuel gas, typically acetylene. A spark ignites the mixture and produces a controlled explosion that propagates down the length of the barrel [7].

Among the traditional thermal spray processes, HVOF and the D-Gun™ are the ones that most closely resemble cold spraying due to their relatively high particle velocities and somewhat more moderate heating of the sprayed particles.

3.1 Advantages

A big advantage of thermal spray processes is the ability to deposit an extremely wide range of materials. Virtually any material that has a stable molten phase can be deposited, and even some materials that do not melt, such as graphite and many carbide or boride

ceramics, can often be co-deposited with another sprayable material to create a composite coating material [7, 8]. Indeed, the ability to create unique composite materials of highly dissimilar raw materials with mixed, layered, or gradational microstructures is another important advantage of cold spray. Another one is that the range of suitable substrate materials is even greater that the range of sprayable materials. In addition to metals, ceramics, glasses, and polymers, thermal spray coatings have been successfully applied to many other substrate materials including wood, concrete, and even paper. This is possible because the thermal energy of a single droplet of molten material is very limited, and if proper thermal management is used during the process, excessive heat of the substrate can be avoided [7]. Conventional thermal spray also offers the advantage of high deposition rates, which are orders of magnitude higher than those of most alternative coating technologies, such as electroplating or vapour deposition, where deposition occurs at the atomic or molecular level. When spray coating objects are very large or difficult to move, the ability to apply coating *is situ* is also an advantage. It should also be noticed that, compared to coating alternatives like painting and electrodeposition, thermal spray is an environmental friendly approach since its effluents are easy to control and to dispose.

3.2 Limitations

The most important limitations of traditional thermal spray techniques are the presence of porosity and oxides in the spray-deposited material, which can significantly degrade the mechanical, electrical, and thermal properties of the coating as compared with to same material in bulk form.

Excessive porosity can also be a problem if the coating is intended to protect the underlying substrate from species that can cause corrosion or other problems [7]. Conversely, high porosity can also be an advantage in some applications like for thermal barriers or for biomaterials where there is a need for high osteointegration. In general low-velocity processes tend to have higher level of porosity in the range of 5-15% volume, and higher velocity processes origin coatings with less porosity (3-8% volume), although it is quite easy to produce more porosity if desirable.

When spraying metals, the reaction of the hot molten metal with oxygen in the ambient atmosphere results in the formation of metal oxide impurities inside the coating. Excessive heating of the spray material can also result in preferential vaporization of more volatile

species in a complex metal alloy, causing a shift in the chemical composition of the coating material when compared to the feedstock material. Processes that minimize heating of the spray material, such as HVOF and D-Gun™, typically result in lower oxide concentrations and minimal changes in alloy chemistry. Also, the controlled inert atmosphere of VPS creates very little or no oxide during the deposition process, however, some changes in alloy chemistry may still occur due to relatively high temperatures in the plasma jet. Another limitation is the introduction of residual stresses. As each molten droplet solidifies and then cools down to room temperature, it undergoes thermal contraction in direct proportion to the temperature change (ΔT) and the thermal expansion coefficient (α) for that material. Since underlying, already solidified material is typically at a lower temperature, the net result is that each successive layer of material is left in a residual tensile stress, and the overall tensile residual stress in the coating steadily increases as subsequent layers of material are added [7, 8]. Indeed, these are the stress that limits the maximum thickness of thermal spray coatings in many instances, since when it rises it reaches a point where the coated layer will either crack or separate from the substrate. A final noteworthy limitation of virtually all thermal spray processes is the simple fact that deposition is limited to surfaces in a direct line-of-sight of the spray gun. This limitation can also be turned to an advantage in some applications where simple masking techniques, such as rubber or metal masks cut to specific shapes, can be used to limit deposition to selected areas of the workpiece surface.

4. The Cold Spray Process

Cold spray as a coating technology was initially developed in the mid-1980s, by Anatolii Papyrin *et al* while studying models subjected to a supersonic two-phase flow (gas + solid particles) in a wind tunnel [7]. These Russian scientists successfully deposited a wide range of pure metals, metallic alloys, polymers and composites onto a variety of substrate materials.

There is a very basic difference between the conventional techniques and the cold spray process. While in the first ones the device requires both thermal and kinetic energy for the coating formation, in cold spray only kinetic energy is used (Figure 10), although in many aspects, a generic cold spray gun (Figure 11) looks very similar to some of the traditional thermal spray devices described earlier.

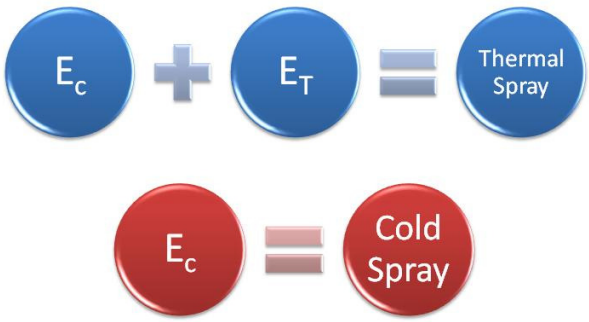

Figure 10 - Basic comparison between the conventional thermal spray techniques and cold spray.

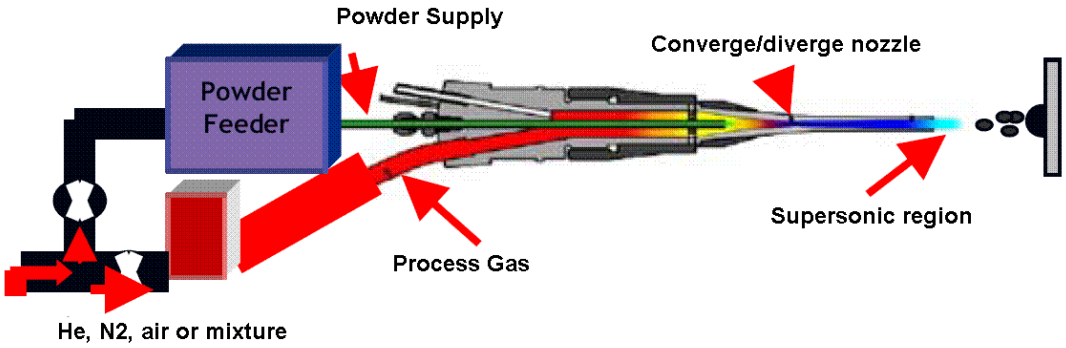

Figure 11 - Schematic diagram of a cold spray gun.

Pressurized gas (generally air, nitrogen or helium) is heated, usually with electrical energy, to temperatures generally in the range of 300-800°C and then passed to a converging-diverging nozzle to create a supersonic gas jet. However, unlike conventional thermal spray processes, the reason to heat the process gas is not to melt the spray material. The gas is heated to increase its velocity to supersonic values, while passing the converging-diverging nozzle [7, 15-21]. The supersonic velocity is reached due to the change of the Mach ($M=v/v_s$, where v is the gas velocity and v_s the sound velocity) number along the nozzle. At the convergent part of the nozzle $M < 1$, in the throat $M = 1$, and in the divergent part $M > 1$. As the gas velocity increases, the gas temperature and pressure decrease, since, due to the "conservation of energy" law, the product "Velocity x Temperature" must be preserved. The relation between the temperature, pressure and velocity, can be observed in Figure 12.

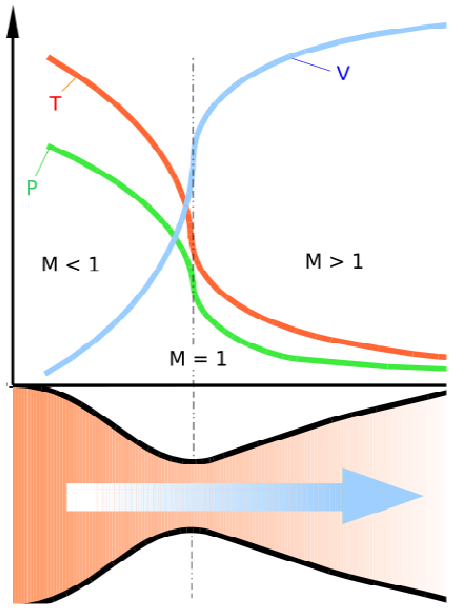

Figure 12 - Diagram of a convergent/divergent nozzle, showing approximate flow velocity (v), together with the effect on temperature (t) and pressure (p) [22].

Since the gas expansion is followed by a temperature decrease, which can in some cases even be below room temperature, the process got the name of "Cold Spray". Figure 13 shows a comparison of approximate process temperature and particle velocity ranges for cold spray and conventional thermal spray processes [7]. Analysing the image, it is clear that cold spray occupies a unique position, offering exceptional low process temperatures combined with high particle velocities.

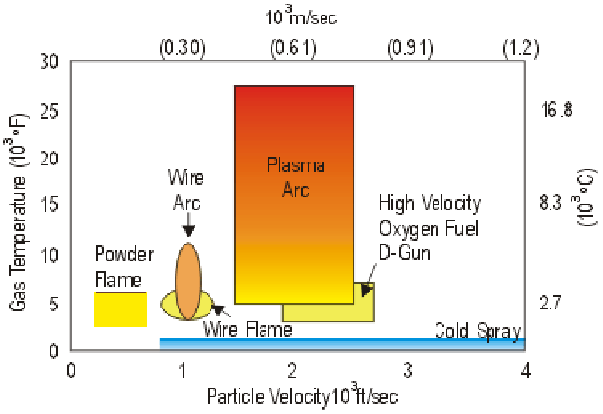

Figure 13 – Comparison of approximate process temperature and particle velocity ranges for several common thermal spray processes and cold spray.

The process uses powder feedstock, in the range of 5-50μm in diameter, that is then injected in the central axis of the cold spray gun. Since the powder particles are only

exposed to the hot process gas for a short period of time, they arrive at the workpiece surface in the solid state, usually far below their melting point. The particles are accelerated to velocities of the order of 500—1200m/s before they impact the surface. If that velocity is sufficient for a given particle/substrate pair, the solid particles plastically deform and flow upon impact, creating an hydrodynamic flow instability at the interface between the incoming particle and the underlying material, which results in bonding at the interface [7, 15-21]. A more detailed discussion of this bonding process will be presented later in this text.

4.1 Advantages

Eliminating the harmful effects of high temperature on coatings and substrates presents significant advantages and new possibilities [7, 18]. As previously discussed, porosity and metal oxide impurities are two important limitations of conventional thermal spray processes, than can be reduced or even avoided in Cold Spray. The greatly reduced level of porosity (<1%) in the cold-sprayed material results from the fact that cold spray is a solid-state process, so there is no splashing. In addition, the “peening” effect of incoming high-velocity particles tends to close the small pores and gaps in the underlying material [7]. The lower content of oxides is due to the cold spray being carried out at much lower temperature and the reaction between the metal and the oxygen in the ambient spray can be greatly reduced or eliminated. Since it’s the presence of a high degree of porosity and oxides that affects the mechanical, electrical, and thermal properties of the sprayed materials, the cold spray process offers again advantages when compared to the conventional thermal spray techniques. Although cold-sprayed metals, in the as-sprayed condition, tend to have low ductility (like the traditionally sprayed metals) due to the high level of plastic deformation inherent to the process and consequent work hardening, since they are porosity and oxide free, a simple post-deposition heat treatment can dramatically improve the ductility [7, 18].

Another potential advantage that the solid-state deposition offers is that the chemistry, phase composition, and crystal (grain) structure of the feedstock powder are preserved in the coating. As referred before, one of the limitations of the conventional thermal spray techniques is that metal alloys that contain multiple elements may experience some shift in their composition due to the preferential volatilization of more volatile elements. And also, the melting/solidification process can dramatically alter the crystal structure or the phase composition compared to the feedstock material. This doesn’t happen in cold spray,

because the particles experience minimal heating, so the initial composition and structure are preserved [7]. This represents a great promise, for example, in the field of nanocrystalline materials, where the challenge as always been to preserve the nanocrystalline size of the crystals after the coating deposition which wasn't possible due to the grain growth resulting from the high process temperatures [23, 24].

Also, opposed to the tensile residual stress state present in traditionally thermal sprayed coatings, limiting their thickness and sometimes leading to cracking or lost adhesion to the substrate, cold sprayed coatings remain under compressive residual stress [7, 8]. As in HVOF and D-Gun™, the very-high-velocity particles in cold spray are very effective in "peening" the underlying material. In addition, since the cold spray particles are deposited at low temperature, there is very little temperature-driven dimensional change.

Like the conventional techniques, cold spray is also a line-of-sight process, which also can be seen as an advantage or disadvantage depending on the application. But in comparative terms the spray pattern of a cold spray gun is more highly focused and allows for easier spraying at very highly localized areas.

4.2 Limitations

Although cold spray can offer significant advantages when compared to the traditional thermal spray processes in selected applications, it also has its own inherent limitations. The fact that the sprayed particles are not melted limits the range of materials that can be cold sprayed and also the range of process-compatible substrates. Unlike traditional thermal spray, cold spray is essentially limited to depositing ductile metals – such as aluminium, copper, steels, nickel-based alloys, etc. – onto metal, ceramic, or other relatively hard substrate materials 7]. This limitation arises from the fact that incoming solid particles must plastically deform upon impact in order to create the hydrodynamic shear instability that binds the incoming particle to the underlying material. For this to occur the spray particle must have enough ductility to allow its plastic deformation and flow, and the substrate must be hard enough to cause the incoming particle to plastically deform. For this reason, brittle materials are not compatible with the cold spray process unless they are co-sprayed with a ductile matrix forming a composite material.

Also cold spray process uses much larger quantities of process gas than traditional thermal spray processes, which can be an issue when a more expensive carrier gas, like helium, is

required to achieve the necessary impact velocities and coating quality. Some preliminary studies indicate that may be feasible to address this issue by capturing and recycling helium. However this greatly increases the cost and complexity of the cold spray system.

In addition, the extensive plastic deformation inherent in the deposition of cold-sprayed metals work hardens the sprayed materials and results in very low ductility of the coating in the as-sprayed condition. While this may be an issue for some coatings, for others it is not a drawback. In other applications, the slightly harder work-hardened coated material may actually be an advantage [7].

Analysing the advantages/disadvantages of the process and the results reported by many authors, it is possible to state that a novel approach to deposit coatings with any given thickness, from particles in the solid state, has been developed [7]. Cold sprayed titanium coatings have high potential for applications in aerospace, corrosive environments, bio-compatible implants, and direct fabrication of titanium products (e.g. near net shape coatings).

5. Cold Spray Process Parameters

As in traditional thermal spray techniques, the film growth rate and final coating properties, in the cold spray process, are determined by several parameters like the impact particle velocity, the spray angle of the gun, the stand-off distance, the molecular weight of the carrier gas, the surface roughness, the powder morphology and distribution, the feeding rate, the particle and gas temperatures, etc. The influence of the most relevant parameters in the deposition efficiency will be described shortly in this section. Coating deposition efficiency is measure as the increase in the coating thickness divided by the number of passes of the spraying gun.

5.1 Particle Velocity

The most important parameter in cold spray process is the particle velocity prior to impact on substrate. For a given material, there exists a critical particle velocity. Only the particles reaching a speed over the critical velocity can be deposited to produce a coating. To better understand this phenomenon lets analyse Figure 14, which shows a typical curve of the induction time as a function of the particle impact velocity. The induction time (or incubation time) represents the time between the beginning of surface treatment by the flow of particles and the beginning of particle adhesion to the surface [17, 25].

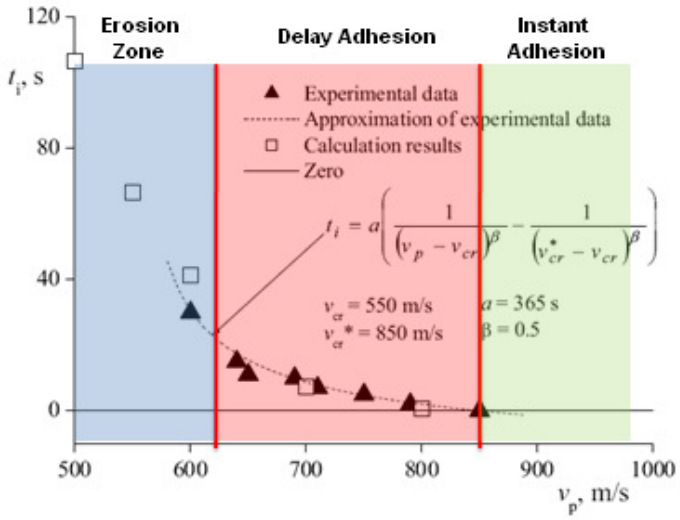

Figure 14 - Deposition delay (induction) time versus the average impact velocity of aluminium particles on a polished copper surface, d_m=30,2μm, φ = 10^{-8}, (mass flow rate of the powder per unit area is 0,06kg/m^2s) [25].

In Figure 14 it is possible to observe three distinct zones of interaction between the particle and the substrate, divided by two values of particle velocity v_{cr1} and v_{cr2}. In the region where the velocity is higher than v_{cr2} (850m/s), represented in green, particles adhere to the initial surface without any delay. When the velocity is between v_{cr1} and v_{cr2} (red) particles cannot adhere instantly to the initial surface. The adhesion starts with some delay (induction time) that corresponds to the time during which the surface state is changed due to its "treatment" by the first impinging particles [25]. The chemical activity of the surface is increased as a result of the creation of an elevated concentration of dislocations in the surface layer. And when these dislocations reach the surface, the places of their exit act as centre of initiation of chemical interaction between the particles and the substrate. There is also the possibility that a certain amount of attached particle material, left on the surface by the rebound particles, will approach the value of activation energy of the substrate with the one of the impinging material. As a result, the activation energy of the particle-substrate interaction decreases. The induction time will increase when the particle velocity decreases since more intensive activation of the surface is required. Also the induction time is inversely proportional to the rate of particle flux in the gas flow. For the third region, area in blue, which corresponds to values of velocity lower than v_{cr1} (550m/s), only erosion occurs, since particles do not adhere to the surface regardless of the treatment time. This is called critical velocity, value for which there is the transition from erosion to coating formation [18, 25].

According to Schmidt *et al* [26], an approximate value of the critical velocity can be calculated as follow:

$$v_{cri} = 667 - 0.014\rho + 0.08(T_m - T_R) + 10^{-7}\sigma_u - 0.4(T_i - T_R) \quad (2)$$

Where ρ represents the particle density, T_m the melting temperature, T_R the reference temperature (293K), T_i the impact temperature and σ_u the yield stress.

5.2 Powder Morphology

A finer particle size distribution will make a powder more suitable for Cold Spray. This is attributed to the fact that gas/particle momentum transfer or particle acceleration imparted by the gas is proportional to 1/d, based on Newton's law and assuming a spherical particle, where d is the diameter of the particle to be accelerated [15, 20]. Consequently, higher acceleration and, therefore, particle impact velocity are to be expected when using a powder with a smaller particle size distribution, as long as the jet Mach number is limited to values below or close to 3. Since the drag force acting on a particle (D) is proportional to the particle drag coefficient (C_D), an increased drag coefficient leads to an increased drag force acting on the particle and thus to a higher particle velocity. This is expressed in Eq. (3), where ρ is the propellant gas mass density, V_{rel} is the relative velocity between the propellant gas and the particle and A_P is the particle projected surface area.

$$D = \frac{1}{2}\rho {V_{rel}}^2 A_P C_D \quad (3)$$

While the friction drag for spherical and non-spherical particles is likely to be similar, the shape form drag of the non-spherical particles will be higher leading to a higher total drag coefficient. As a result, a larger drag force will be applied to the non-spherical particles, promoting higher particle velocity at the end of the acceleration zone of the nozzle, as measured [20, 27].

The rationalization that smaller and irregular shape powders are beneficial to cold spray was verified using a numerical model developed for the cold spray process and validated with laser diagnostic tools [20].

Another important aspect about the morphology of the powder is that a non-spherical particle with rough surfaces and irregular features will have a different contact behaviour during impact. Ajdelsztajn et al. [28] have shown that the localized shear deformation at

the particle boundaries during impact promotes an intimate contact between particles and helps the formation of a particle/particle metallurgical bond. This will be enhanced by a larger surface area of the irregular particle morphology (non-spherical), increasing particle/particle interaction during the deformation process. Also, the irregular morphology will increase the stress concentration during impact due to the fact that the load cannot be uniformly distributed as it may be observed in spherical particles [28]. The stress concentration at the surface of the particle can facilitate the occurrence of a localized shear deformation and also the disruption of the surface oxide layer present in metallic powders, leading to an intimate contact between particles.

5.3 Powder feeding rate

Varying the mass flow rate at which the powder is fed into the carrier gas stream changes the coating thickness as seen in Figure 15. Coating thickness increases linearly with feeding rate until a maximum value is reached for which there are too many particles impacting the surface of the substrate resulting in excessive residual stresses causing the coating to peel [29]. This can be compensated by the increase of the gun's travel speed.

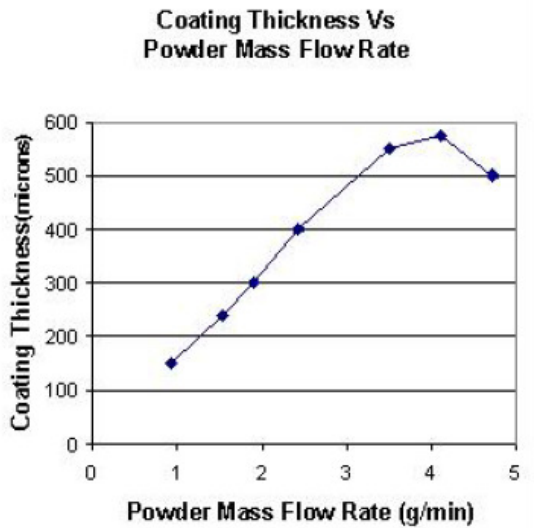

Figure 15 - Coating thickness as a function of powder mass flow rate [29].

5.4 Spray Angle

Figure 16 and

Figure 17 show the influence of spray angle on the relative deposition efficiency of copper and titanium respectively. It is possible to observe that the maximum efficiency was

obtained at spray angles ranging from 80 to 90° for copper, and 70 to 90° for titanium [30]. In such angle range, the spray angle as practically no influence in the deposition efficiency. Although, if we further decrease the spray angle outside this interval, the deposition efficiency will also decrease till an angle below which no particle deposition occurs (40° for copper and 50° for titanium).

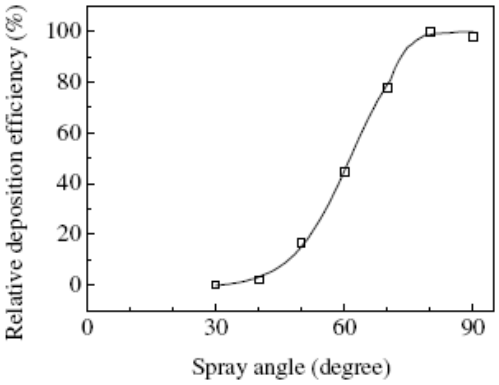

Figure 16 – Effect of spray angle on the relative deposition efficiency of copper (15-37μm) [30].

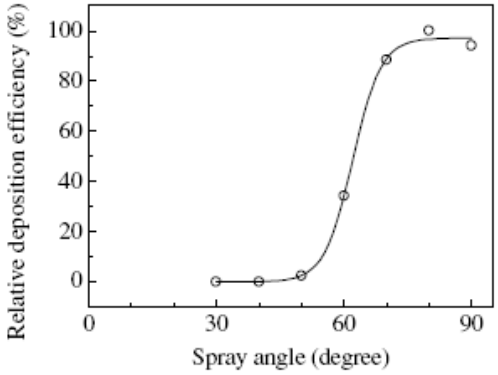

Figure 17 - Effect of spray angle on the relative deposition efficiency of titanium (37-44μm) [30].

As said before, only particles that have a velocity higher than the critical velocity at normal impact are deposited on the substrate. With the decrease in spray angle, the normal component of velocity will also decrease, and when its value becomes less than the critical velocity the particle will not deposit on the substrate.

In the impact of a particle at off-normal angle, the particle impact velocity can be decomposed in a normal component and a tangential one relative to the substrate as shown in the next figure.

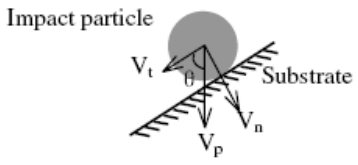

Figure 18 - Decomposition of particle impact velocity at spray angle of θ [30].

The normal (V_n) and tangential (V_t) velocities can be expressed as:

$V_n=V_p \sin\theta$

$V_t=V_p \cos\theta$

Where V_p is the particle impact velocity and θ is the spray angle between the nozzle axis and substrate surface. V_n decreases with a decrease in θ from 90° to zero.

Regarding the dependency of the relative deposition efficiency on spray angle, the spray angle can be divided in three angles ranges: maximum deposition angle range, transient angle range and no deposition angle range (Figure 19).

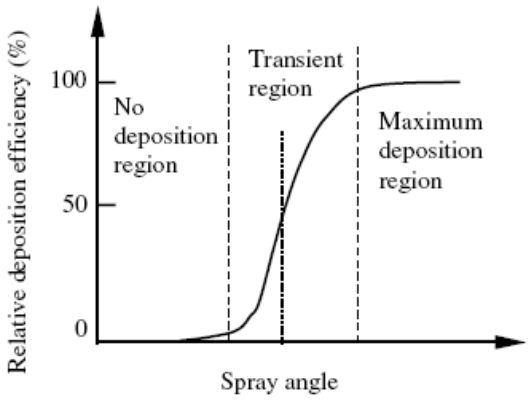

Figure 19 – General schematic diagram of the dependency of relative deposition efficiency on spray angle [30].

Also, a larger powder particle size distribution leads to a larger velocity distribution which will affect the range of the maximum deposition angle and transient angle, which can be observed in

Figure 16 and

Figure 17. The titanium particles have a larger maximum deposition range and a smaller transient range due to their narrower size distribution compared to the copper particles [30]. The spray angle also influences the coating microstructure, since the particles deformation direction in the coating changes with the spray angle. The particles flow direction is approximately perpendicular to the particle approaching direction.

5.5 Stand-off distance

Before explaining the influence of the stand-off distance in the cold spray process it is important to define bow shock phenomenon. It is known that the particle velocity

increases outside the nozzle and that the particles may lose velocity during the flight, although this velocity can be further reduced due to the shock wave resulting from the previous particles impacting the substrate (Bow Shock) [15]. Therefore at small stand-off distances, when the strength of the bow shock is high, deposition performance is reduced. While at large stand-off distances, when the bow shock has disappeared, deposition can continue unhindered. Analysing

Figure 20, it is possible to observe three distinct stand-off regions: First (1) the small stand-off region, where the presence of the bow shock adversely affects deposition performance; Second (2) the medium stand-off region, where the bow shock has disappeared and, if the gas velocity remains above the particle velocity (positive drag force), the deposition efficiency continues to increase; and Third (3) the large stand-off region, where the gas velocity has fallen below the particle velocity (negative drag force), and the particles begin to decelerate. For optimal deposition performance, the stand-off distance should be set within Region 2 [15].

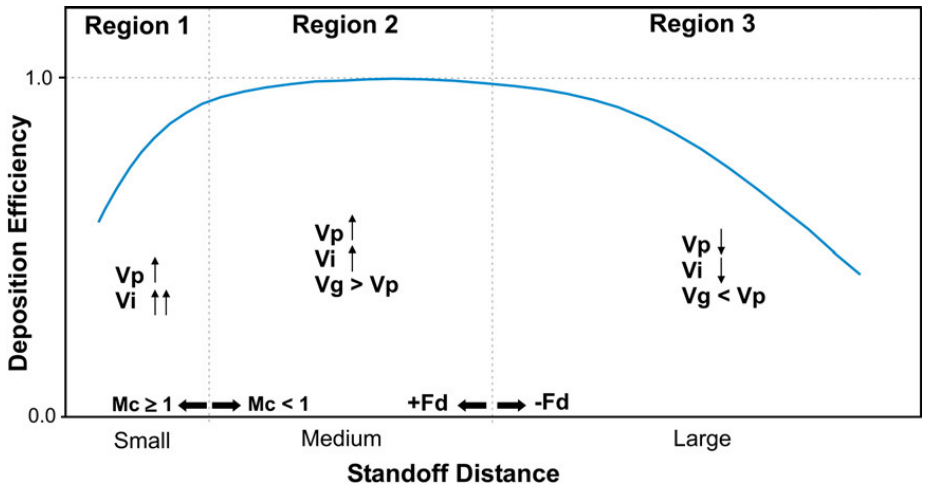

Figure 20 - Chart showing the effect of stand-off distance on deposition efficiency. Here F_d is the drag force, M_c is the centreline mach number, V_g is the gas velocity, V_i is the particle impact velocity and V_p is the in-flight particle velocity [15].

5.6 Particle, substrate and gas temperature

According to Schmidt et al [31], the coating quality can be further improved by increasing the initial temperatures of particle and substrate. That is because higher initial particle temperatures result in lower critical velocities since the material is already softer at higher temperatures and that less kinetic energy is needed to heat particle surface areas

by plastic deformation. Moreover, heat conduction will be less effective due to lower temperature gradients, which leave more time for diffusion and bonding.

Temperature influences the process of cold spray in different manners. Firstly, with increasing stagnation temperature the velocity of the process gas is increased, and accordingly also is the particles impact velocity. Secondly, it is known that elastic and plastic properties of materials depend upon temperature. The materials temperature can be changed by using a higher gas temperature or by pre-heating the powder and/or the substrate. Increased materials temperature could enhance thermal softening which is important for the bonding mechanism and also potentiate chemical reactions that may also induce adhesion.

Also, the use of a gas with a lower molecular weight will have the same effect has increasing the gas temperature, since it also increases the particles velocity. The same happens when increasing the gas pressure.

5.7 Surface Roughness

Richer et al. [32] refer that the surface roughness resulting from different grit types only affects the deposition efficiency for the first few layers of particles impinging on the substrate. Defining the initial bonding mechanism at the substrate/coating interface thus becomes important.

One of the suggested theories for the bonding mechanism of cold sprayed coatings is associated to mechanical interlocking of the impinging powder particles to the substrate surface. It is thus reasonable to assume that an increased substrate roughness would further enhance bonding as it presents a greater array of nooks and recesses in which Cold Spray particles can be lodged. These particles are then subjected to additional compaction as successive particles impact on the substrate. This phenomenon is illustrated in Figure 21.

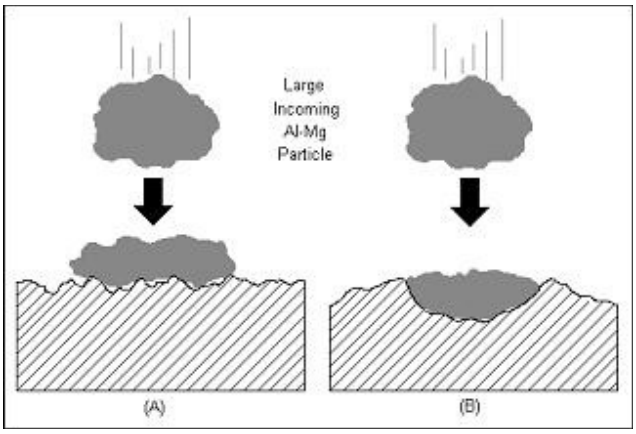

Figure 21 - Schematic representation of large Al-Mg particles impinging a substrate surface with (a) low surface roughness and (b) high surface roughness [33].

For surfaces with low roughness, the first particles to impact would have little surface area to which to bind, resulting in weaker bond strengths. These particles thus have a greater difficulty adhering to the substrate, resulting in an initial reduction in deposited mass.

Other authors [34] report that the bond strength is higher for an as-received (Ra≈2,6μm) substrate than for a grit-blasted one (Ra≈3.5μm), being 37 and 32 MPa respectively. This could be due to the work hardening associated to the grit-blasting treatment of the substrate surface, therefore making it more difficult for the sprayed coating to bind to the substrate.

6. Bonding Mechanisms in Cold Spray

The actual mechanism by which the solid particles deform and bind during cold spray is still not well understood. On one hand, Sansoucy et al. [35], Dykhuizen and Smith [36] and Morgan et al [31] have proposed a cold spray bonding mechanism based on an effect called mechanical anchorage, in which no melting or metallurgical reactions were observed. This theory holds at low temperature and pressure (which means low particle velocity). On the other hand, Schmidt et al. [31] have proposed another bonding mechanism based on adiabatic shear instability, which occurs at sufficiently high particle impact velocity with extensive thermal softening of particles. Thus, this theory holds at high temperature and pressure. It also explains the transition from erosion to cold spray adhesion, the behaviour of powder deposition efficiency and the existence of an incubation time [17].

It is well established, however, that the feedpowder particles and the substrate/deposited material undergo extensive localized deformation during impact. This causes disruption of the thin (oxide) surface films and enables an intimate conformal contact between the

particles and the substrate/deposited material. Intimate conformal contact of clean surfaces combined with high contact pressures is believed to be a requirement for particles/substrate and particles/ deposited material bonding [7, 8, 22, 23, 32 - 39]. With the beginning of the impact, a strong pressure field propagates spherically into the particle and substrate from the point of first contact, Figure 22(a). The pressure gradient at the gap between the colliding interfaces generates a shear load, which accelerates the material laterally and thereby causes localized shear straining. When the impact pressure, and the respective deformation, are high enough, this shear straining leads to adiabatic shear instabilities. This means that thermal softening is locally dominant over strain and strain-rate hardening, which leads to a discontinuous jump in strain and temperature and an immediate breakdown of stress. The viscous flow in this region generates an out-flowing material jet with material temperatures close to the melting temperature, Figure 22(b).

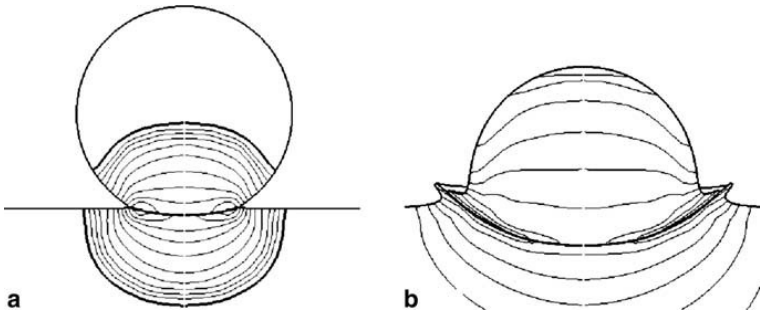

Figure 22 – Pressure field during impact (a), jetting (b) [31].

This hypothesis is supported by a number of experimental findings such as:

(a) a wide range of ductile (metallic and polymeric) materials can be successfully cold-sprayed while non-ductile materials such as ceramics can be deposited only if they are co-cold-sprayed with a ductile (matrix) material;

(b) the mean deposition particle velocity should exceed a minimum (material-dependent) critical velocity to achieve deposition which suggests that sufficient kinetic energy must be available to plastically deform the solid material and/or disrupt the surface film;

(c) the particle kinetic energy at impact is typically significantly lower than the energy required to melt the particle suggesting that particle/substrate and particle/deposited material bonding is primarily, or perhaps entirely, a solid-state process. The lack of melting is directly confirmed through micrographic examination of the cold sprayed materials.

6.1 Coating formation in Cold Spray

The bonding process for the kinetic spray procedure is a complex particle–particle and particle–substrate interaction, as described above. The basic coating formation arises from a transformation of the kinetic energy of the particles into mechanical deformation and thermal energy, which occurs rapidly, on the order of 10^{-7} s.

An understanding of how the coating builds can be obtained by dividing the growth process into four basic phenomena (Figure 23). During the initial stage, a thin film of particle material (a so called monolayer) is deposited on the substrate. This stage is characterized by a direct interaction of particles with the substrate and depends very much on the degree of surface preparation and on the properties of the substrate material. The initial stage includes the time of surface activation (induction time) during which erosion instead of deposition can occur. In the second stage particle deformation and re-alignment occurs. A layer of finite thickness is build up. As densification increases, the material at the point contacts is displaced, contact area grows in size and material flows into the interparticle voids, which is a kind of “peening” effect. The third stage is characterized by the formation of a metallurgical bond between particles and void reduction. Stage four corresponds to further densification and work hardening (due to the peening effect) of the coating [31].

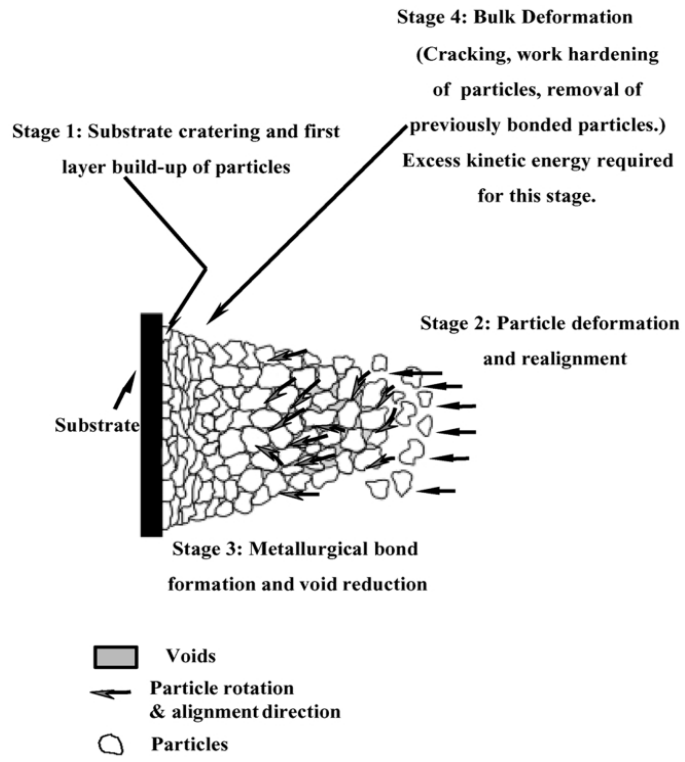

Figure 23 - Stages of coating formation in the cold spray process [31].

7. Cold Spray Applications: State-of-the-Art

The current state-of-the-art is rapidly changing. To date, most cold spray depositions have been made with nitrogen and have focused mainly on aluminium, copper, zinc, and other pure materials due to the limitations in the powder material's ability to plastically deform under certain deposition conditions [7]. Ceramics typically do not plastically deform to the extent that metallic materials do, making difficult the deposition of 100% ceramic materials at low temperature.

Since the "cold gas" technology is rather recent, no large-scale, commercial applications have yet established themselves in the broader thermal-spray marketplace. Although, due to such properties as dense, oxide-free coatings, a multitude of new applications now present themselves which were not feasible using conventional processes, establishing cold spraying as a viable technology.

The Cold Spray process is potentially applicable to corrosion-resistant coatings (zinc and aluminum), dimensional restoration and repair (nickel, stainless steel, titanium, and aluminum), wear-resistant coatings (chromium carbide – nickel chromium, tungsten

carbide – cobalt, and tungsten copper), electromagnetic interference (EMI) shielding of components and structures, and field repair of components and systems [40].

At the moment, cold spraying already being applied in different areas, like automotive manufacturing in copper metallizations for junction blocks, deposition of NdFeB permanent magnetic particles compacted in an iron matrix for electric machines (conductors, soft magnetic materials and permanent magnets), deposition of zinc onto steel for selective galvanizing at specific locations of a structure and spraying of high-purity iron over ceramic moulds for rapid tooling repair [41]. Cold spray is also being used to apply a copper thermal management layer on a critical rocket engine component [42]. Cold-spraying was also used to impart electrical conductivity to polymer surfaces by the apparent "implantation" of graphite particles, and resulting change in surface conductivity of thermoplastic polyolefins by as much as six orders of magnitude [43]. Other envisioned applications include the development of cold welding and repair processes for aluminium body structures and placement of brazing materials [41].

Up until recent, hard wear-resistant coatings using cold spray processes have not been explored in depth. Although some work has been done with CrC-Ni, CrC-NiCr and WC-Co compositions, additional efforts are needed in order to define cold spray process composition capabilities and additional opportunities in applying wear- and erosion-resistant coating materials [7].

8. Objective and Experimental Planning of the Thesis

As said before, the main goal of this project is to optimize the cold spray process in order to obtain a fully dense titanium coating into a 7075-T6 aluminium alloy. To lead to optimization, the first step is to determine which factors and which interactions between them are important in affecting the response. For that, different process parameters will be varied and then the pair with the highest deposition efficiency will be chosen. Finally, analysing the obtained results, we will try to better understand the mechanisms leading to the bonding formation between the coating and the substrate.

It is important to plan the work in order to obtain the requested information with the minimum number of experiments. And when the goal is to observe of how *K* factors influence a process and how these factors interact with each other, the optimal

experimental strategy is the 2^K factor analysis [44]. This design allows exploring a chosen area of the experimental domain and finding the promising direction for the optimization.

Due to its simplicity, a complete matrix 2^K of factorial experiments doesn't require the use of specialized software to build it or to analyse its results. In this design, each factor is only study at two levels and the experiments include all the combinations of each level of a factor with all the levels of the other factors. The matrix will include 2^K rows and *K* columns, which correspond to the K factors under study. Each column starts with the sign -, and the signs – and + will alternate with a frequency of 2^0 for X_1, 2^1 for X_2, 2^2 for X_3, and successively till X_k where the signs will alternate with a frequency of 2^{k-1}. The sign – corresponds to the minimum values and the sign + to the maximum values of the factor.

The variables that affect the cold spray process were previously described in chapter 4, and from these we will determine K factors.

The available cold spray apparatus is a KINETIC®4000 (Cold Gas Technology, Ampfing, Germany), it has a maximum operating pressure of 40bar, temperature of 850°C and it is limited to the use of nitrogen as the carrier gas, so the characteristics of the process gas can be eliminated as a variable. In addition, KINETIKS® 4000 is equipped with a pre-chamber of 120 mm in length connected to the gun nozzle where powders are heated up by the hot gas for a longer time.

Also, from the literature cited before [30], it can be seen that if we maintain the spraying gun at 90° the deposition efficiency will be maximum, so this variable can also be eliminated. We have then the gas temperature, the gas pressure, the powder feeding rate, the stand-off distance and the surface roughness as possible factors. This would mean 2^5=32 experiments.

As said before, most of authors believe that the surface roughness affects the adhesion of the first layers of the coating [32] and consequently the bond strength [33]. To make it simpler this parameter will be eliminated as a factor and, after the optimum conditions are chosen, adhesion tests will be carried for different substrates preparations. We have now 2^4=16 experiments.

In order to reduce this number of experiments to 8 a previous test to determine the optimum stand-off distance was preformed. The values chosen were 20mm, 40mm and 60mm and the results are shown in Figure 24Figure 25 and Figure 26. Comparing the images

we can discard the distance of 60mm since there is a gap between the coating and the substrate, which means that there is almost no bonding between them. Regarding the other two, we can see that for the distance of 20mm the coating is more irregular and easily pealed during the cut operation, making the distance of 40mm the optimal spraying distance for the cold spray deposition of titanium with KINETICS® 4000.

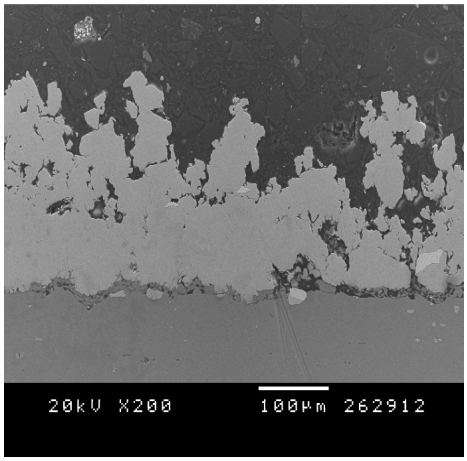

Figure 24 – SEM micrograph of titanium deposited into aluminium 7075-T6 at the standoff distance of 20mm.

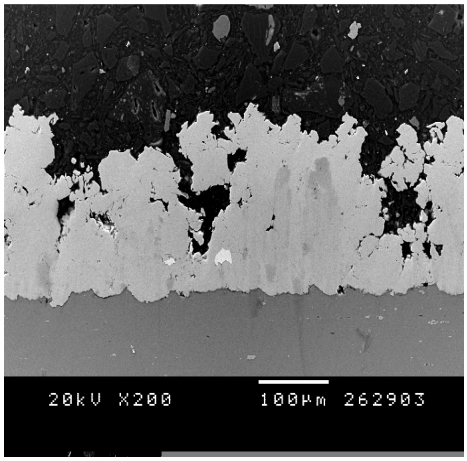

Figure 25 - SEM micrograph of titanium deposited into aluminium 7075-T6 at the standoff distance of 40mm.

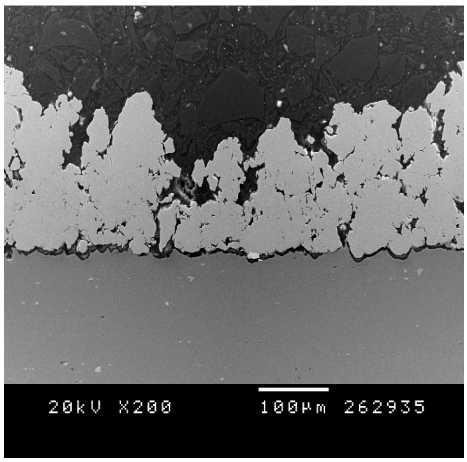

Figure 26 – SEM micrograph of the titanium deposited onto aluminium 7075-T6 at the stand-off distance of 60mm.

We have then three variables: gas temperature, gas pressure and feeding rate of the powder. These factors are shown in Table 1 together with the experimental domain. Alternating the levels of the factors we reach the experimental matrix that it is represented in Table 2. Figure 27 represents the combined experimental domain for the three factors where the set of parameters evaluated in this project are marked in red.

Table 1 - Factors and experimental domain.

Factors	-	+
X1 - Temperature	600-700°C	700-800°C
X2 - Pressure	30-35bar	35-40bar
X3 - Feeding Rate	2-4rpm	4-6rpm

Table 2 - Matrix of experiments.

	X1	X2	X3	Result
1	-	-	-	Y1
2	+	-	-	Y2
3	-	+	-	Y3
4	+	+	-	Y4
5	-	-	+	Y5
6	+	-	+	Y6
7	-	+	+	Y7
8	+	+	+	Y8

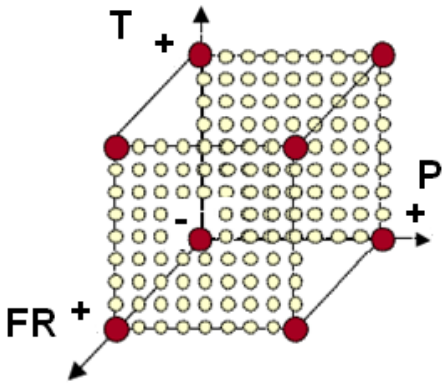

Figure 27 - Cube that represents the experimental domain. At the vertices, in red, are represented the chosen experiments.

The results from the eight experiments can be combined in order to determine: the influence of the three principal effects, of three effects of interaction of two factors and of the effect of the interaction of the three factors in the final result. The order in which each element is either added or subtracted is given by the matrix of interactions represented in Table 3. This matrix will allow to determine which parameter influences more the final result.

Table 3 – Matrix of interactions.

	T	P	Rpm	T x P	T x Rpm	P x Rpm	T x P x Rpm
1	-	-	-	+	+	+	-
2	+	-	-	-	-	+	+
3	-	+	-	-	+	-	+
4	+	+	-	+	-	-	-
5	-	-	+	+	-	-	+
6	+	-	+	-	+	-	-
7	-	+	+	-	-	+	-
8	+	+	+	+	+	+	+

Decided the temperature, pressure and feeding rate intervals, and fixing the gun passages at 2 in order to allow surface activation, the other process parameters were set at:

Table 4 - Fixed process parameters.

Accelerating and Carrier Gas	Nitrogen
Pre-heating Temperature	400°C
Standoff Distance	40mm
Gun speed	500mm/s
Angle of Deposition	90°

9. Results and Discussion

9.1 Powder Characterization

The powder used for the deposition of the titanium coating was a microcrystalline Commercial Purity titanium Grade 1 powder from Mechanomade® obtained by ball milling. It was previously known that the powder had good fluidity and it was further characterized according to its particle size distribution and morphology.

9.1.1 Particle size distribution

The study of the particle size distribution was made through a Laser Diffraction Particle Size Analyser Beckman Coulter LS 13320. Analysing Figure 28 it is possible to observe that the differential volume has a Gaussian distribution. The statistic of the particle size distribution can be found in Table 5, where it can be seen that 80% of the particles are between 40.34 and 94.01 μm with a mean size of 58.37 ± 1.42 μm.

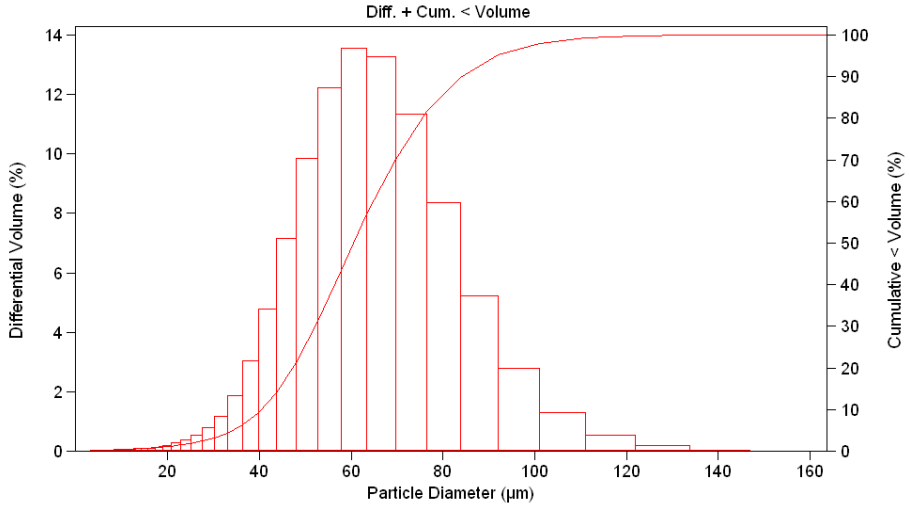

Figure 28 - Particle size distribution of the titanium powder. The differential volume is expressed in bars and the accumulated volume in a continuous line.

Table 5 - Statistics of the particle size distribution of the titanium powder.

Parameters	Result
Mean particle size	58.37 µm
Diameter correspondent to 10% accumulated volume	40.34 µm
Diameter correspondent to 50% accumulated volume	60.53 µm
Diameter correspondent to 90% accumulated volume	84.01 µm

This powder presents a size bigger than the ideal size (5-45µm) but it is still inside the range to be deposited through cold spray. Also, due to its wide size distribution (22-90µm), the particles may present a high difference in their impact velocity, since fine and coarse particles, by having different weights, will impact on the substrate at different velocities because they can't reach the same kinetic energy. This can be a problem regarding reproducibility once the results may be different depending on which powder fraction will impact the substrate at that point.

9.1.2 Structural characterization by Scanning Electron Microscope (SEM)

The analysis of the powder's morphology via SEM allows to observe that the particles size distribution coincides with the results obtained via laser diffraction (Figure 29). It can be seen that the powder particles are very angular and have a very irregular form, which is consistent with the powder's fabrication method and an advantage for the cold spray process since the irregular particles reach higher velocities [20, 27].

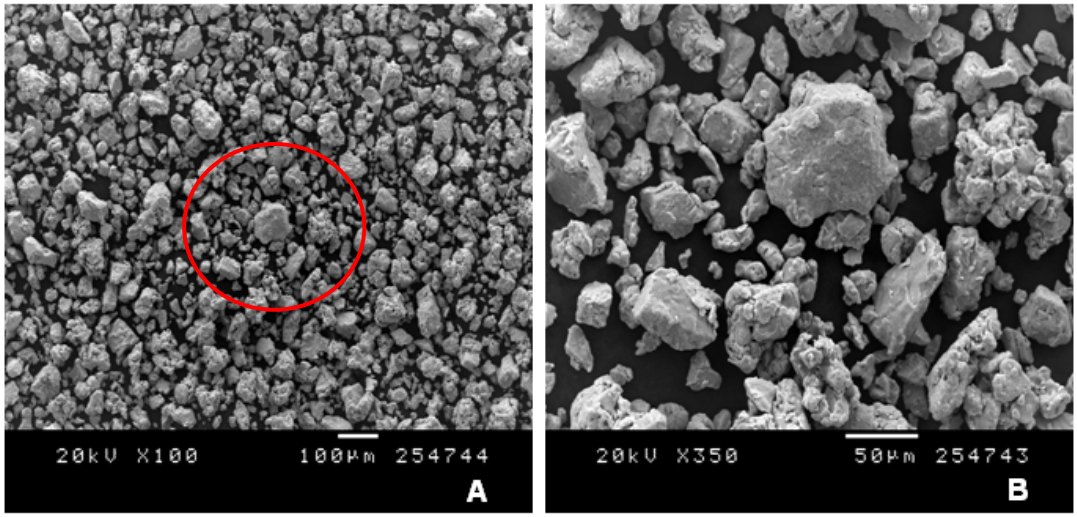

Figure 29 – A) SEM microphotograph of the free surface of the Titanium Mechanomade® powder. B) Close-up of the underlined area.

9.1.3 Structural characterization by X-Ray Diffraction

The X-ray analysis of the powder is shown in Figure 30. The diffraction peeks correspond to the ones characteristics of pure titanium (the peek lines are represented in red in Figure 30) what confirms that this powder is indeed pure titanium. The peeks are well defined and very narrow with indicates that the powder is highly crystalline.

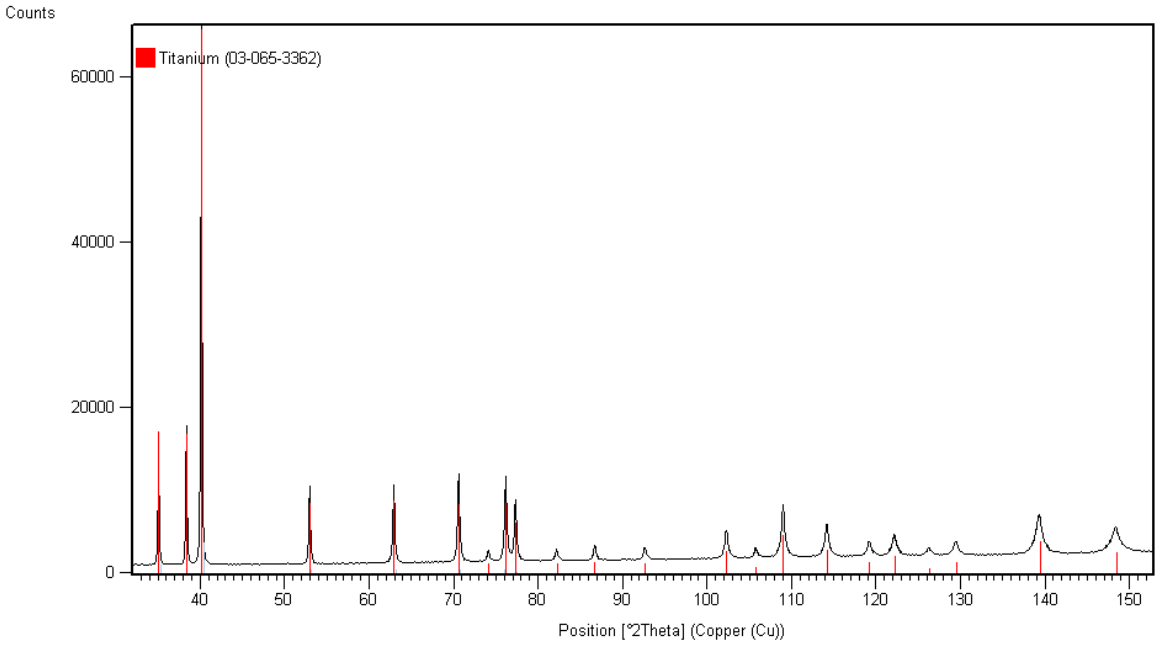

Figure 30 – X-ray spectrum of the titanium powder (black) combined with the line peeks for pure titanium (red).

9.2 Substrate Characterization

The material used as substrate was, as said before, the 7075-T6 aluminium alloy. The powder deposition was conducted in samples with 50x20x5mm.

In Figure 31 is represented this material microstructure, revealed after etched with Keller's reagent for 20 seconds. It is possible to distinguish between recrystallized grains (clear) and uncrystallized grain fragments that appear dark as a result of precipitation at boundaries of $MgZn_2$ [45].

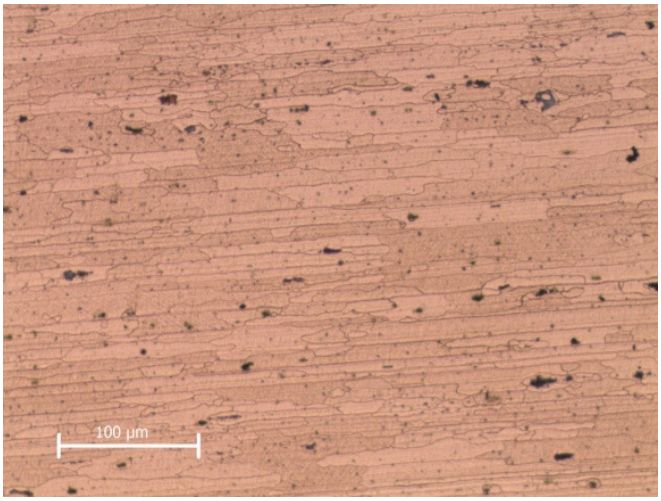

Figure 31 – Optical micrograph of aluminium 7075-T6, material used as substrate.

A more detailed characterization was conducted with the Transmission Electron Microscope. The resulting images are shown in Figure 32. In this figure, A represents a Selected Area Electron Diffraction (SAED) analysis of the area shown in B. The spots pattern indicates that the analysed area is a single crystal, which means that the micrograph corresponds to a region inside an aluminium grain. Also, the bright ring in the centre of A indicates the presence of precipitates, in this case $MgZn_2$, that correspond to the dark dots present all over the micrograph B.

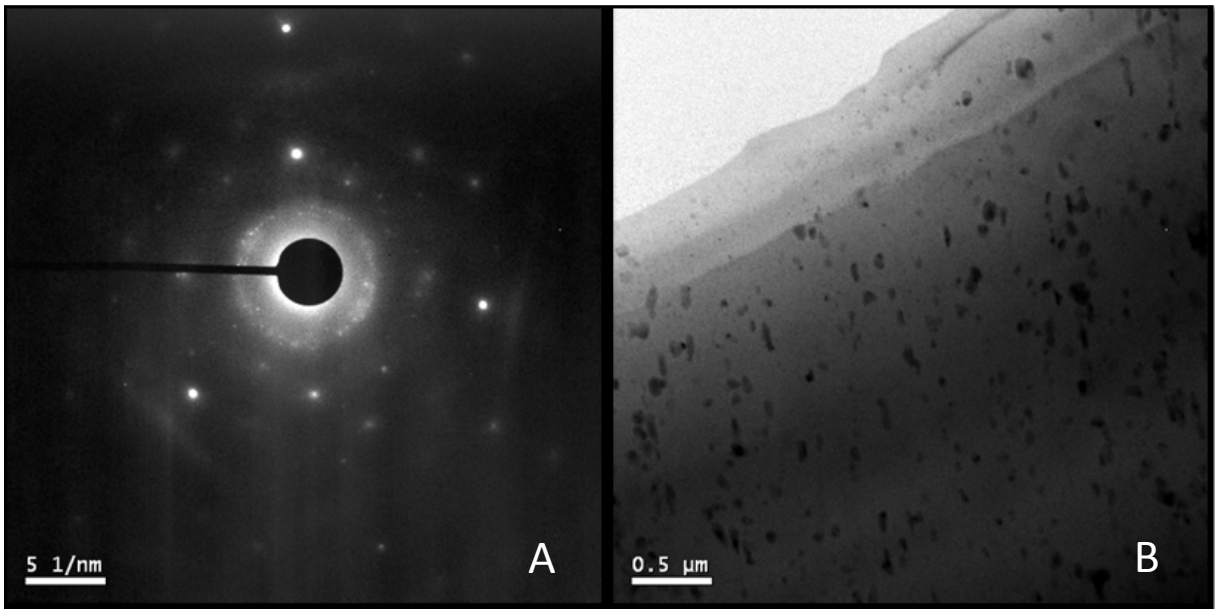

Figure 32 – A) Selected area electron diffraction (SAED) pattern and B) TEM micrograph of the aluminium substrate.

For a confirmation of the alloy's mechanical properties two tests were conducted: tensile test and Vickers micro-hardness. The values obtained were in agreement with those predicted in the material data sheet (Annex 1).

9.3 Coatings Characterization

The coatings obtained with the different combinations of deposition parameters presented before with numbers 1 to 8, are shown in Figure 33 with the respective numeration. The coatings were characterized according to their thickness (Figure 34), porosity (

Figure 35) and hardness (Figure 36).

Observing Figure 33 it is possible to distinguish two different zones. In the top region from the surface to the boundary, there are a lot of large pores. On the other hand, in the inner region from the boundary to the substrate the coating has a dense microstructure. It is also possible to observe that the size of the pores decreases with the increase of the depth from the surface towards the boundary. This happens due to the "peening" or tamping effect previously explained.

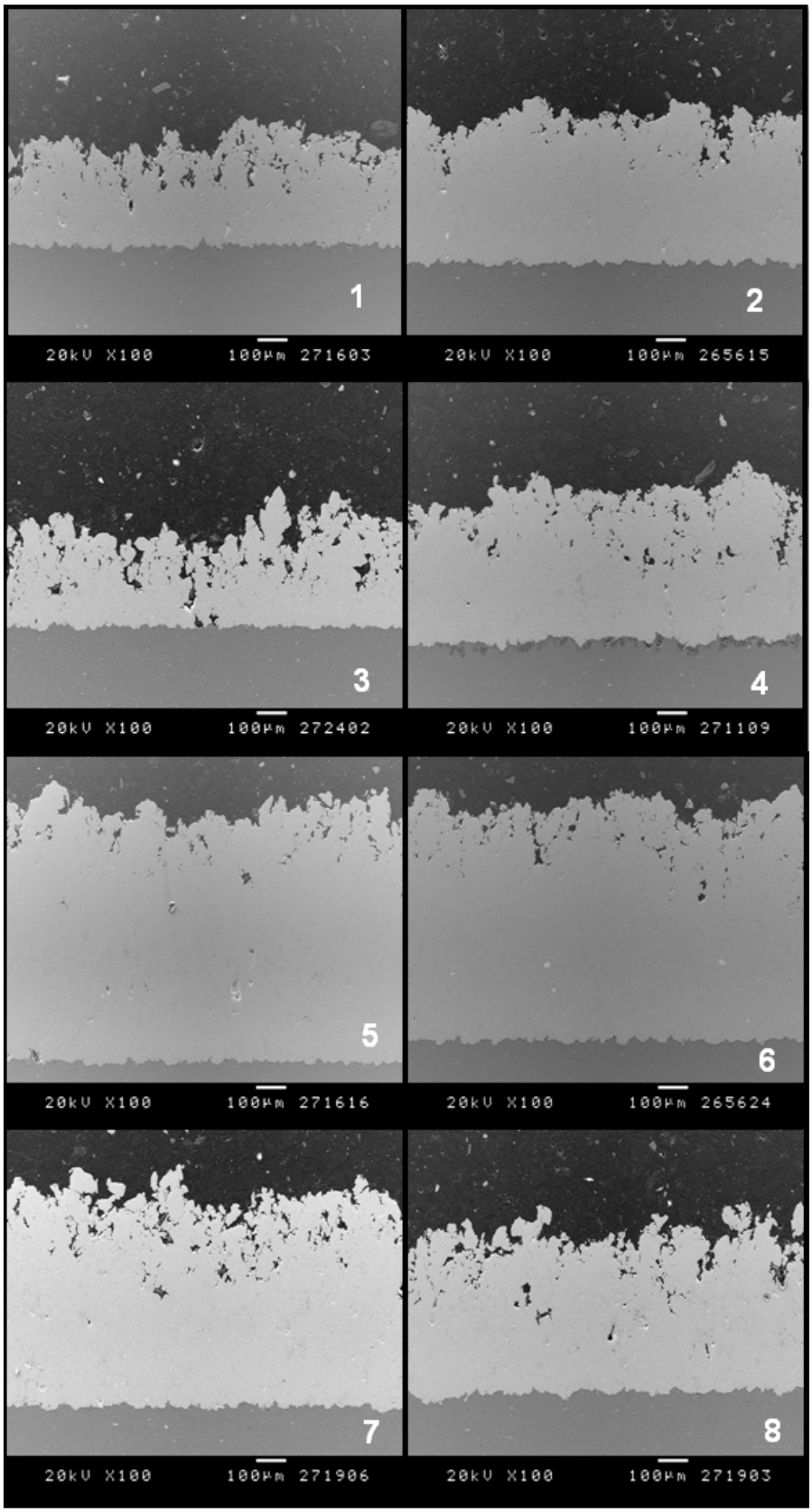

Figure 33 - SEM micrographs of the titanium coatings obtained with the parameters set from 1 to 8 respectively.

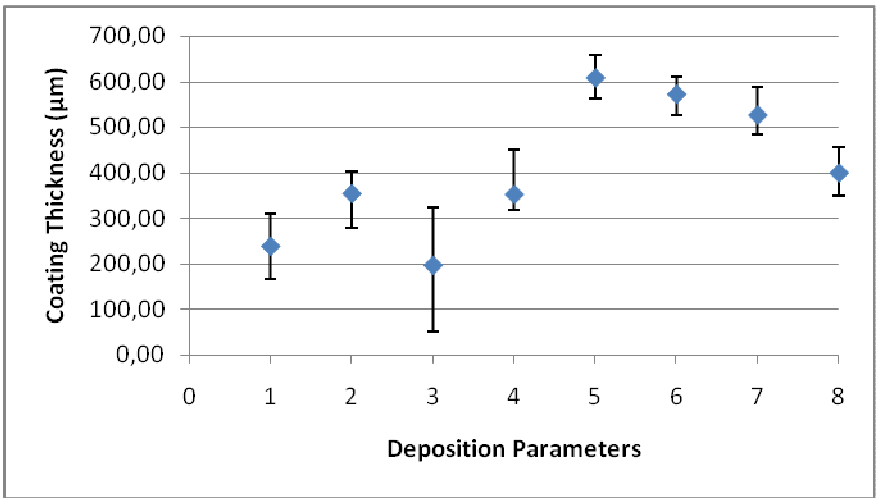

Figure 34 - Graphic that illustrates the coating thickness obtained for each set of parameters.

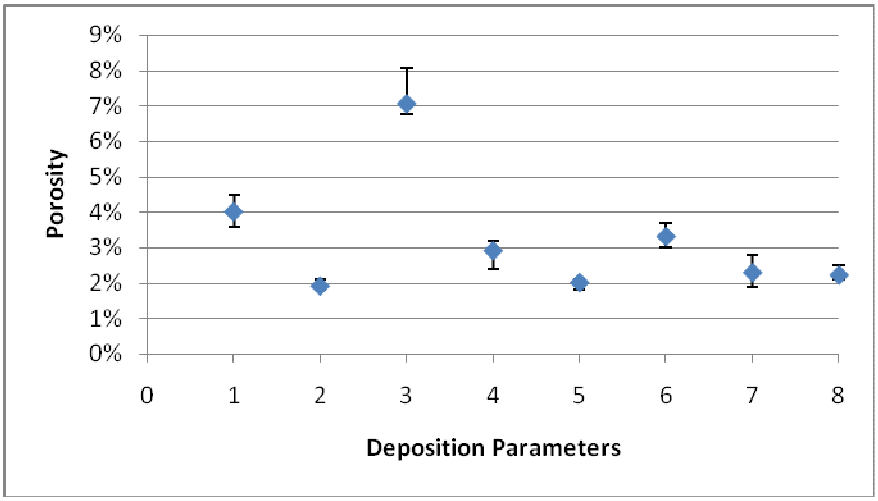

Figure 35 - Graphic that illustrates the coating porosity obtained for each set of parameters.

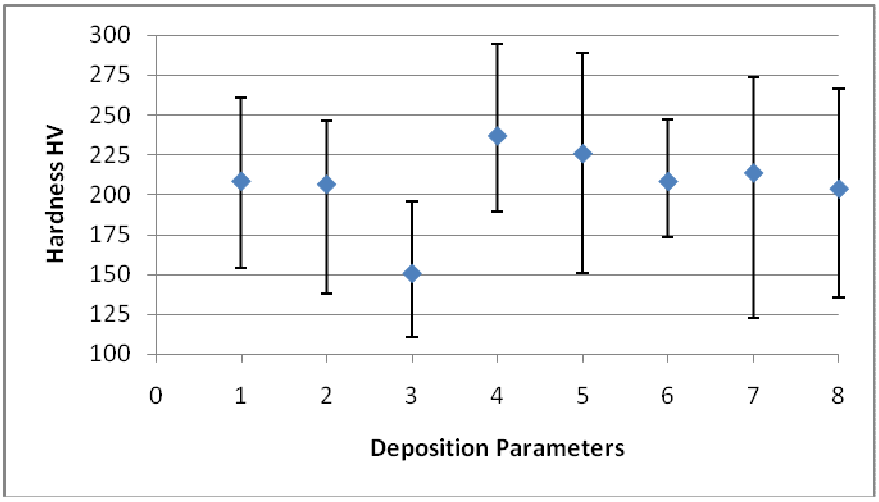

Figure 36 - Graphic that illustrates the coating hardness obtained for each set of parameters.

From the analysis of Figure 33 andFigure 34, it can be observed that the coating thickness increases with the rising of the powder feeding rate. This was expected since almost the double amount of powder is used in the process. It also increases with the gas temperature for a feeding rate of 2-4rpm because a higher number of particles can reach the critical velocity and consequently bond to the substrate increasing the coating thickness. The same happens when pressure rises. On the other hand, for a feeding rate of 4-6rpm this is not verified maybe due to the accentuated rebound effect cause by the higher amount of particles (nearly the double) impacting the surface, which may interfere with the trajectory of incoming particles preventing them from impacting the substrate, or loose velocity, and consequently not bond, reducing the final coating thickness. The same is verified for a higher pressure.

The porosity level (Figure 35) was measured through the Max Inspector Programme. It is important to notice that not all the voids present in Figure 33, 1 to 8, are pores. Due to the high particle size distribution, in the same coating are present particles with a size of 20μm and particles with size of 100μm, which have a different behaviour during the flight and impact the substrate at different velocities. This results that some particles, which didn't have enough energy to bond to their neighbours and should only cause erosion, get trapped by the arriving particles and incorporate the coating. And when preparing the sample for microstructural analysis, during the polishing operation, these particles get detached leaving a void. This problem may origin results different from the real ones. According to the images, the porosity decreases with the rise of temperature, as expected, since the particles plasticity increases resulting in a denser coating. However, the pressure influences negatively the porosity level since it increases it. The porosity at 30-35bar varies from 2 to 4%, while at 35-40bar it varies from 2 to 7%. It can then be considered that in the highest interval, the particle velocity is so high that the rebound effect increases the porosity (either due to the incoming particle not bonding or due to detaching a poorly attached particle) and so the erosion domain is reached. It is though important to refer that this porosity is all concentrated in the top region of the coating, and if this region was later mechanically removed, the coating would be virtually 100% dense[1]. In the case of different feeding rates the obtained results are not comparable since, at higher feeding rate, the coating thickness is much higher decreasing the ratio (porosity area)/(coating area) which is how the programme calculates the porosity.

[1] Figure 48 shows a CPT coating (Coating 12) after removal of the external porosity layer.

The coating hardness (Figure 36) is sensibly the same for all the coatings except for number 3 where it is quite low probably because of the high amount of voids that allow particle displacement during measure. The average value of 210HV is much higher than the Vickers value for bulk titanium (≈122HV). This can be explained by the deformation-hardening effect caused by the particles that impact over the already bonded particles introducing beneficial compressive stresses in the coating.

The influence of the parameters on the coating properties can be confirmed by the factorial analysis represented in Table 6.

Regarding the coating thickness, the parameter with highest effect is the feeding rate since increasing it from 2-4 to 4-6rpm increases it in average 241μm, followed by the temperature which increases it 27μm and finally the pressure, which its increase decreases it 74μm. This values are in accordance in the results expected at the beginning of this experiment, since a pressure increase should result in a denser coating and consequently in a smaller thickness.

The rise of temperature increases the coating thickness for a feeding rate of 2-4rpm, while it decreases it for a feeding rate of 4-6rpm. The interaction of the temperature and the feeding rate is then of big importance. When both the temperature and feeding rate are increased, at a fixed pressure, the coating thickness decreases 108μm. This supports the statement that at high feeding rate and high temperature, the rebound effect overcomes the increase of plasticity and, instead of contributing to the growing of the coating, it causes erosion. The same reasoning can be made for the interaction of the other parameters.

For the porosity, according to the obtained images and, consequently, the factorial analysis, it is once again shown that it increases with the pressure for the previous explained reason. And, as expected, it decreases with the temperature. For the feeding rate the result may be deceiving as said before. The decrease in the porosity by the interaction of the temperature and pressure is due to increase of the particle plasticity overcoming the velocity increase.

Finally, the hardness was virtually the same for all the coatings (high error range) so its results should not be considered.

Table 6 – Calculation of the parameters effect on the coating thickness, porosity and hardness. Factorial analysis.

	Effect	Thickness	Porosity	Hardness
T	(- y1 + y2 - y3 + y4 - y5 + y6 - y7 + y8) / 4	27.1	-1.3%	14.2
P	(- y1 - y2 + y3 + y4 - y5 - y6 + y7 + y8) / 4	-74.6	0.8%	-11.1
Rpm	(- y1 - y2 - y3 - y4 + y5 + y6 + y7 + y8) / 4	241.3	-1.5%	12.3
T x P	(+ y1 - y2 - y3 + y4 + y5 - y6 - y7 + y8) / 4	-12.8	-0.9%	24.0
T x Rpm	(+ y1 - y2 + y3 - y4 - y5 + y6 - y7 + y8) / 4	-108.6	1.9%	-27.9
P x Rpm	(+ y1 + y2 - y3 - y4 - y5 - y6 + y7 + y8) / 4	-52.7	-1.2%	2.7
T x P x Rpm	(- y1 + y2 + y3 - y4 + y5 - y6 - y7 + y8) / 4	-32.8	0.2%	-20.2

Analysing the coatings structure and their properties it is possible to exclude the coatings number 1, 3, 4, 5, 7 and 8 due to the high amount of pores and to the very irregular surface. It is then possible to state that the best combinations of parameters are number 2 and 6 and their main difference is in the coating thickness. Coating number 2 presents a thickness in the order of 400µm and coating number 6 in the order of 600µm. Comparing these values to the ones obtained by conventional thermal spray techniques, which are in the order of 200µm for higher number of gun passages, it is possible to say that the optimum condition is number 2, since its thickness is more than sufficient to form a protective coating for the required application, and the 600µm of coating 6 become too high making it less economically viable. However, the high thickness that cold spray easily achieves suggests this process as a potential alternative to laser cladding with the advantage of avoiding the heat affected area.

9.4 Wipe Tests

In order to better understand the particle bonding process and the concept of critical velocity and incubation time, the so called “wipe tests” were conducted for two extreme conditions with the same feeding rate: number 1 for the slower particle velocity, and number 4 for the highest particle velocity. This test consists in moving rapidly a substrate through the spray jet. The results are shown in Figure 37 - SEM micrograph of the Wipe Tests realized for the two opposite velocity conditions with the same powder feeding rate. A and B correspond to parameter set number 1 and C and D to set number 4.

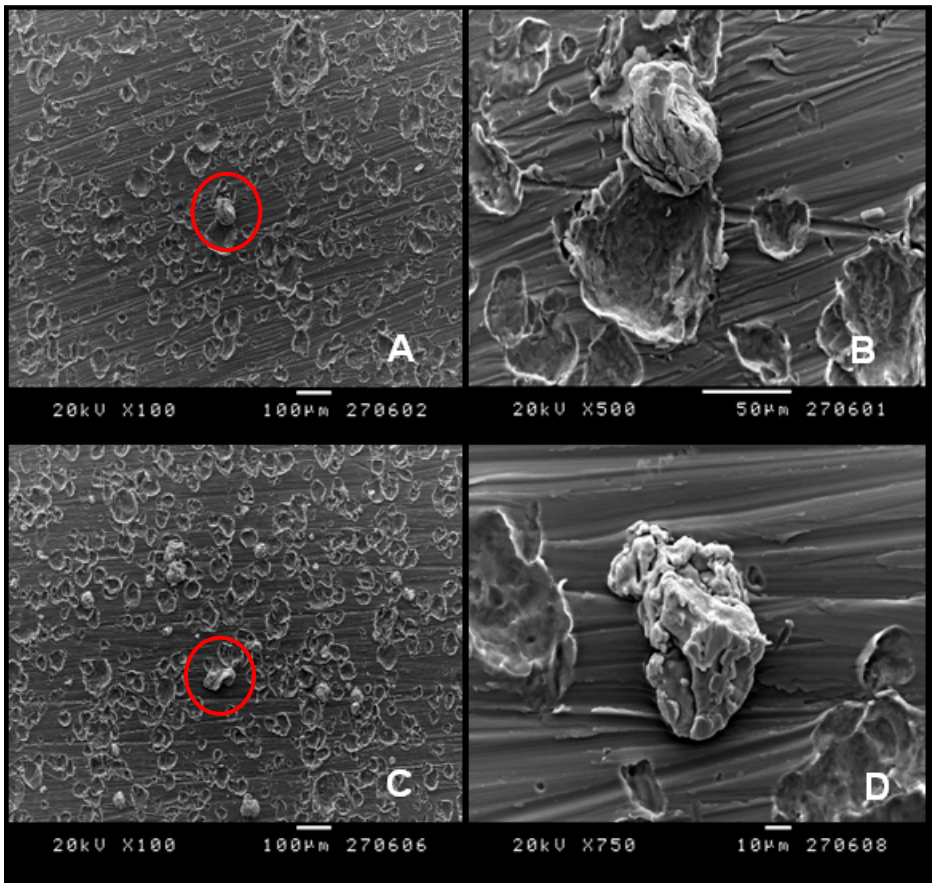

Figure 37 - SEM micrograph of the Wipe Tests realized for the two opposite velocity conditions with the same powder feeding rate. A and B correspond to parameter set number 1 and C and D to set number 4.

It can be seen that for the lowest velocity the gun first passage results mainly in erosion that leads to surface activation, and very few particles bond to the surface (Figure 37 A and B). When the velocity is increased to the value of condition number 4 (Figure 37 C and D), erosion is also present but the number of particles bonded to the substrate is much higher, suggesting that the surface activation occurs faster. From this images it is also possible to observe that there is only particle deformation (no melting) supporting the argument that this process occurs in the solid-state.

9.5 Further analysis of the selected coating

In order to verify the aluminium/titanium bonding strength and the hardness profile of the area surrounding the interface a nanoidentation test was preformed in a Nano Indenter® XP system (Systems Corporation). The 75 nanoidentations (matrix of 5x15) were conducted at constant load of 15mN and the results can be seen in Figure 38. The zero value represents the interface zone, and the negative distance corresponds to the substrate while the positive corresponds to the titanium coating.

The hardness of the aluminium is in agreement with the value of the material data sheet (Annex 1). Although it can be seen a slight increase with the approximation to the interface due to the hardening effect introduced by the constant bombing of particles. In the area right next to the interface this value drops due to a small thermal softening of the aluminium, which has low melting temperature, resulting from the high release of energy during the shock of the first particles. The hardness value at the interface is not high enough to allow saying that the bonding is very strong, but it is also not to low since it is in the same order as the aluminium, revealing that the bonding will be good. The hardness for the titanium coating is, as seen before, much higher than the bulk value due to the tamping effect. The hardness decreases with the distance to the interface since the amount of particles impacting on the already bonded ones also decreases, weakening the peening effect.

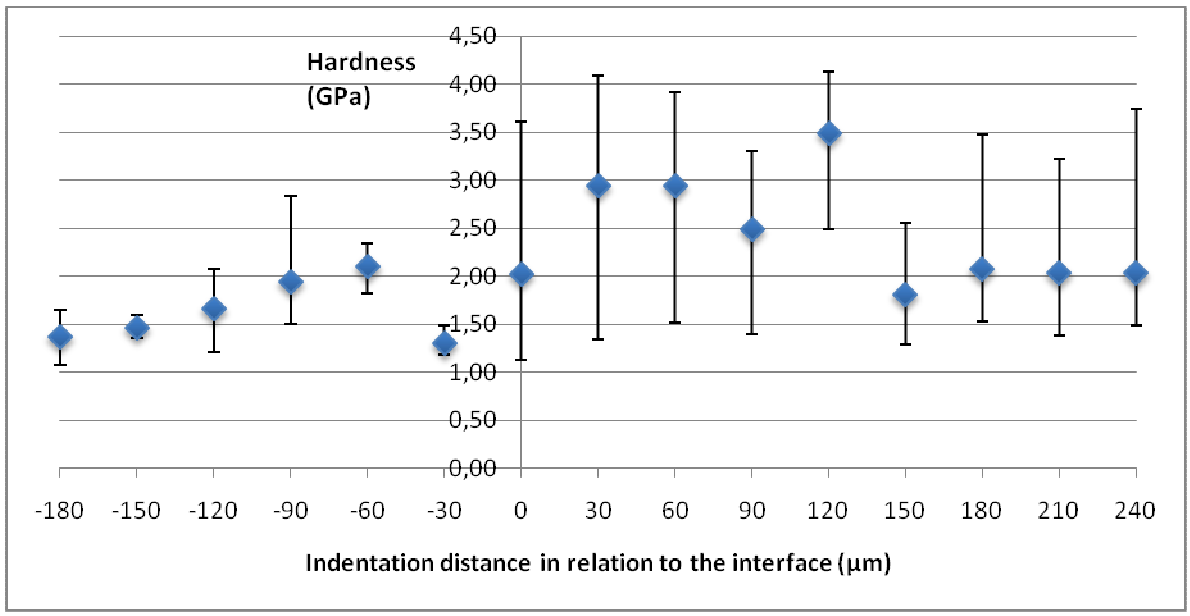

Figure 38 - Nanoidentation profile obtained for the sample number 2.

Besides the logical explanation for the titanium's coating hardening resulting from the successive impact of particles, another possibility needed to be explored: the reaction of nitrogen with titanium. Above 600°C titanium reacts with nitrogen and forms titanium nitride (TiN), which hardness is around 2500HV, value that is not desirable [42]. In order to confirm if the titanium was still pure, an XRD test was preformed.

Analysing the resulting spectrum (Figure 39) it is possible to observe that the purity of the powder maintains and that there are no N2 present, confirming that the time that the powder stays over 600°C is so short that doesn't allow the reaction to occur.

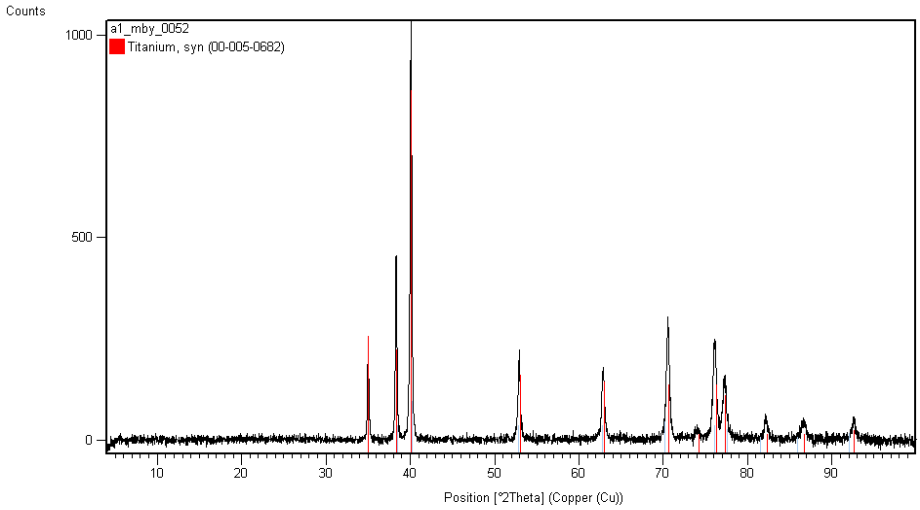

Figure 39 - X-ray spectrum of the coating number 2 (black) combined with the line peeks for pure titanium (red).

Figure 40 represents the coating microstructure after etching. It is possible to observe once again the powder's wide size distribution: particles of 15µm mixed with particles of 70µm. Also the pore size, in the order of 20/30µm, could easily be a void left by a smaller particle that was trapped by the bigger particles, since this represents a zone close to the interface and there should be no pores present. This also may justify the wide hardness distribution, once when the indentation is preformed in the centre of a smaller particle the value is higher than in the centre of a bigger particle. Also the particle displacement due to it being merely trapped represents an obstacle to a good analysis.

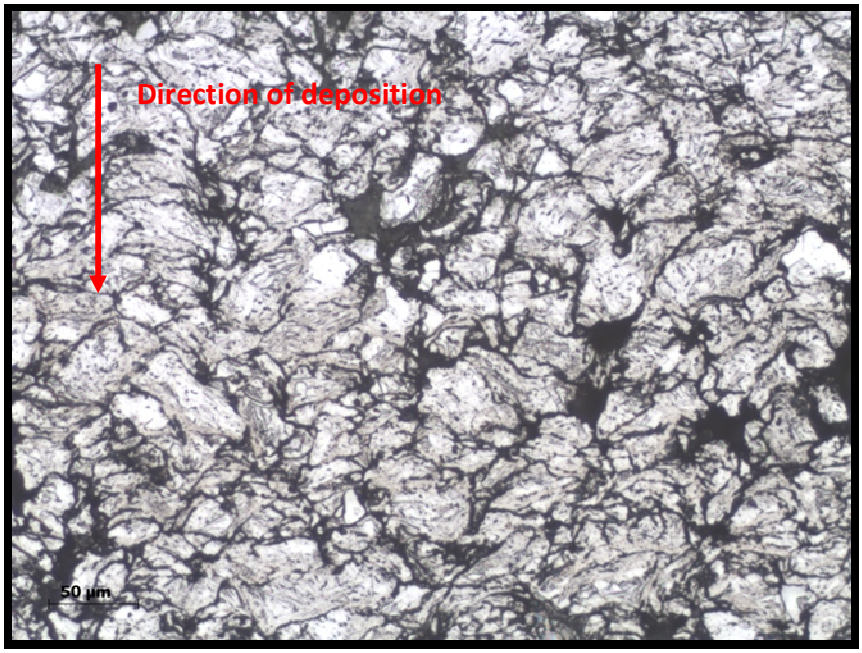

Figure 40 - Optical micrograph of the coating number 2 microstructure after etched with Keller's reagent.

Through the SAED pattern shown in Figure 41 A, it can be seen that the titanium coating is polycrystalline, with crystallite size around a few micrometers. Micrograph B illustrates that some grains have a columnar shape, while others have a more equiaxial morphology. This is surprising because this columnar structure is characteristic from the conventional thermal spray techniques, due to the preferential growth in the direction of the temperature gradient. But since it was observed in the wipe-tests that there was not fusion, at least at a micro scale, it is most likely that these columnar grains correspond to the formation of dislocations cells as reported by Kim et al [47]. The presence of a high amount of dislocations in B may support this hypothesis and confirm that the titanium particles were subjected to high deformation resulting in their hardening, as it was suspected by the hardness values. Such amount of dislocations agrees with the occurrence of the so called adiabatic shear instabilities supported by many authors.

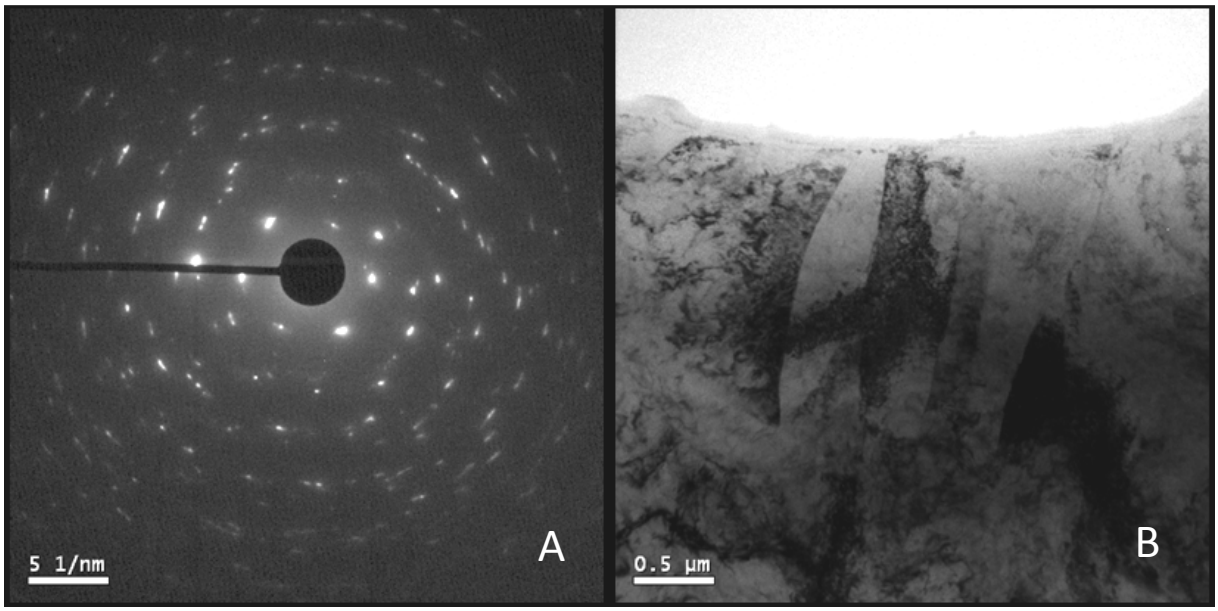

Figure 41 - A) SAED pattern and B) TEM micrograph of the titanium coating.

In order to better understand the bonding process, the TEM analysis of the interface area was also conducted. In Figure 42 A shows the SAED pattern corresponding to interface area represented in B, where one can see the titanium zones, filled by dislocations, mixed with the aluminium areas with their characteristic precipitates. The elemental analysis of different regions indicated a composition gradient of the two elements which indicates that solid-state diffusion as indeed occurred. The presence of an amorphous zone that could indicate a localized fusion, as reported by Xiong et al [38], was not found, which doesn't mean that is not present since it is in the order of a few nanometres. Further investigation should be conducted.

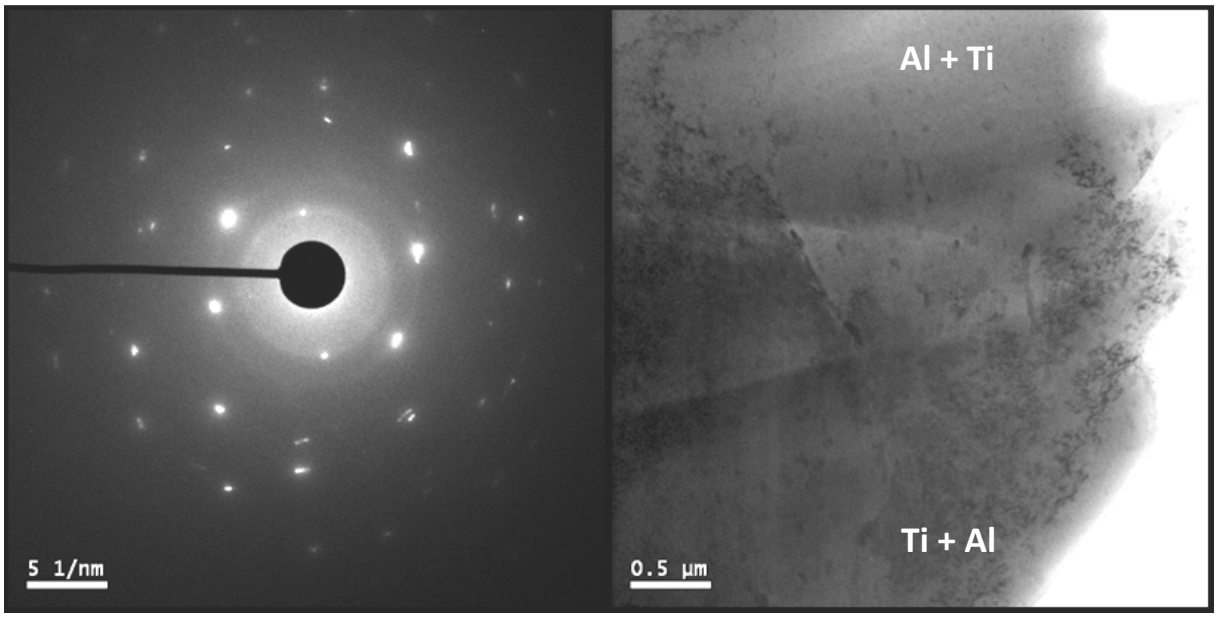

Figure 42 – A) SAED pattern and B) TEM micrograph of the interface aluminium/titanium coating

9.6 Optimization

This wide size distribution that results in particles badly bonded between them, and sometimes merely trapped, is the main reason to the high number of voids and the non-uniformity (both hardness and morphology) of the coating. In order to further optimize the process, a powder with a narrower size distribution should be used. So, to analyse the importance of the particle size in this process, the previous powder was sieved to two groups: one containing the particles between 40-60µm and the other the ones between 22-40µm. Then the feeding rate was maintained at 2-4rpm, the temperature at 750°C and two different pressures were used 35-40bar and 30-35bar.

The resulting microstructures are shown in Figure 45 for 40-60µm and figures 44 and Figure 46 for 22-40µm. The coatings properties are represented in

Table 7.

It can be seen that, thanks to the sieved powder, all the coatings present a more uniform structure with less voids and porosity. When comparing the results for both powder groups, the coatings with higher particle size are rougher and a bit thicker, but again the hardness is less uniform. The denser structure resulting from the smaller particle size, together with

its uniformity, makes the size distribution between 22-40µm the best, of the ones tested, for cold spray.

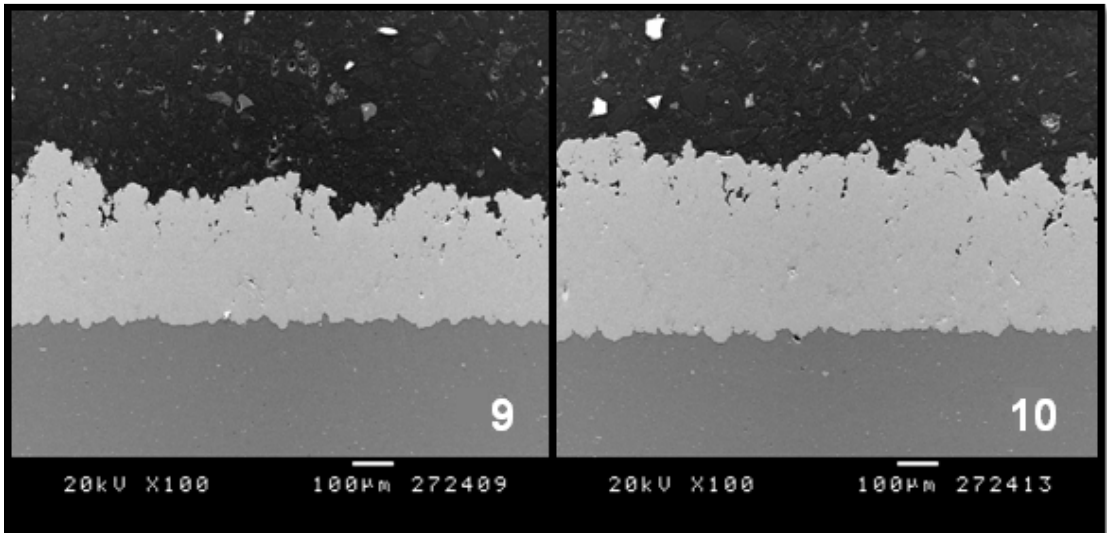

Figure 43 - SEM micrograph of the titanium coating after the powder was sieved and using the fraction 40-60µm. Number 9 corresponds to a pressure of [35,40]bar and 10 to [30,35]bar.

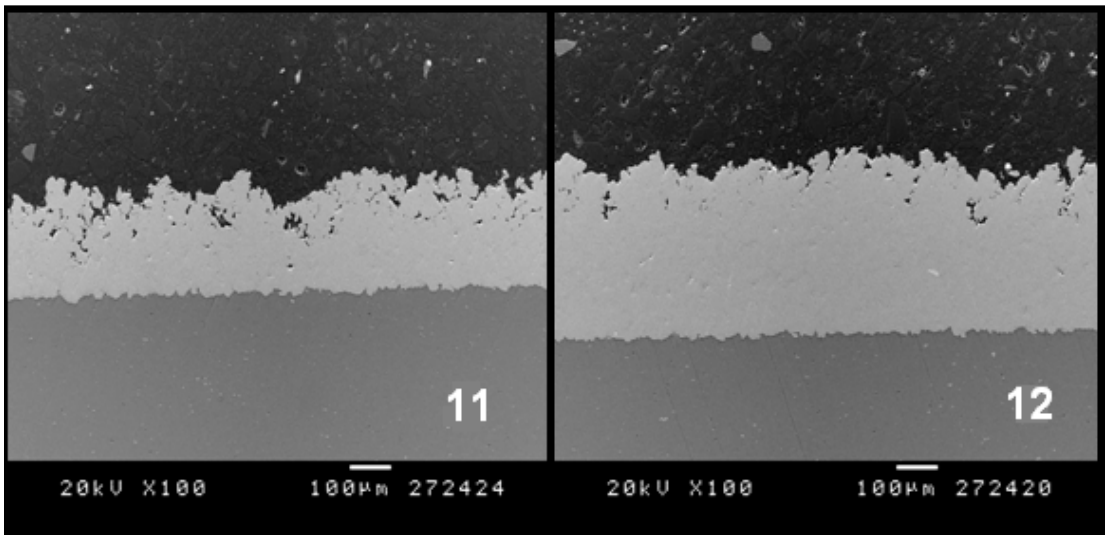

Figure 44 - SEM micrograph of the titanium coating after the powder was sieved and using the fraction 22-40µm. Number 11 corresponds to a pressure of [35,40]bar and 12 to [30,35]bar.

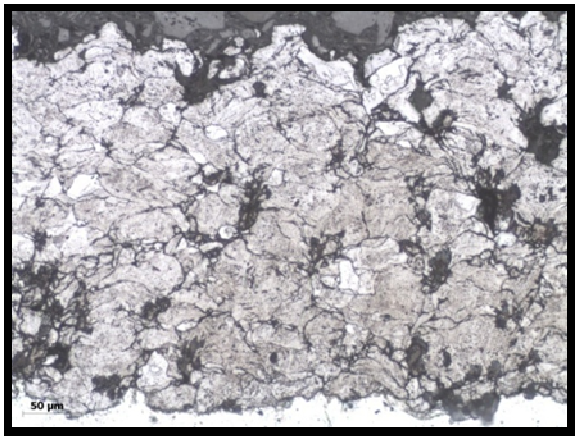

Figure 45 - Optical micrograph of the coating number 10 microstructure after etched with Keller's reagent.

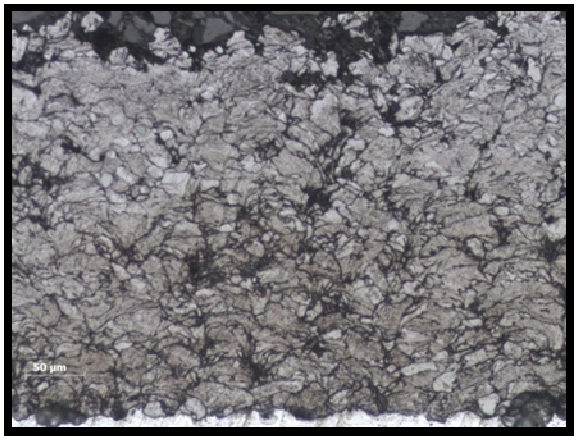

Figure 46 . Optical micrograph of the coating number 12 microstructure after etched with Keller's reagent.

Table 7 - Coating properties for the optimized conditions.

Parameters	Coating Thickness (µm)	Hardness (HV)	Porosity (%)
9	254±50	254±35	1.1±0.1
10	317±35	246±29	0.9±0.1
11	204±32	232±26	1.6±0.1
12	311±25	240±20	0.7±0.1

And once again, comparing the two used pressures, the highest pressure results in a lower coating thickness and in higher porosity, proving that the 30-35bar is the ideal value for the deposition of titanium onto aluminium substrates. Having this in mind, slightly modified adhesion tests, but following the ASTM C-633 standard [48], were conducted in order to determine the bonding strength. The test consists of gluing a cylindrical coated specimen with a resin to an uncoated sand-blasted specimen, as it can be seen in Figure 47. The obtained results are shown in Table 8.

Figure 47 – Set-up for the adherence test.

Table 8 – Adhesion test results for the conditions 10 and 12.

Set	Tensile strength (MPa)	Average σ_S (MPa)
10	32.94	34.3
	34.62	
	35.27	
12	39.21	33.4
	31.50	
	30.17	

The optimum bond strength for a coating is given whenever the failure occurs between the glued surfaces (coated and non-coated surfaces). The used glue resists approximately 70MPa and none of the titanium coatings was able to endure such value. All the coatings exhibited adhesive failure since their rupture was by the substrate/coating interface. The tensile strength average value is very close for both the subjected coatings and it is over the 30MPa, normal value for the plasma-sprayed titanium coatings. However, the values vary between 30MPa and 39MPa, and this last value is a very good result. So, further optimization should be conducted in order to dislocate the average tensile strength value closer to 40MPa.

Once the main goal is to reach a fully dense coating, further optimization was conducted by removing all the porous area. Figure 48 shows coating number 12 after the removal of the external porous layer. The resulting thickness was 240 ± 2µm and the porosity was reduced to 0.05%. The coating presented a superficial hardness of 281 ± 40 HV. This value is higher than the previous result for coating 12 since there is more resistance to deformation because the coating is more compact.

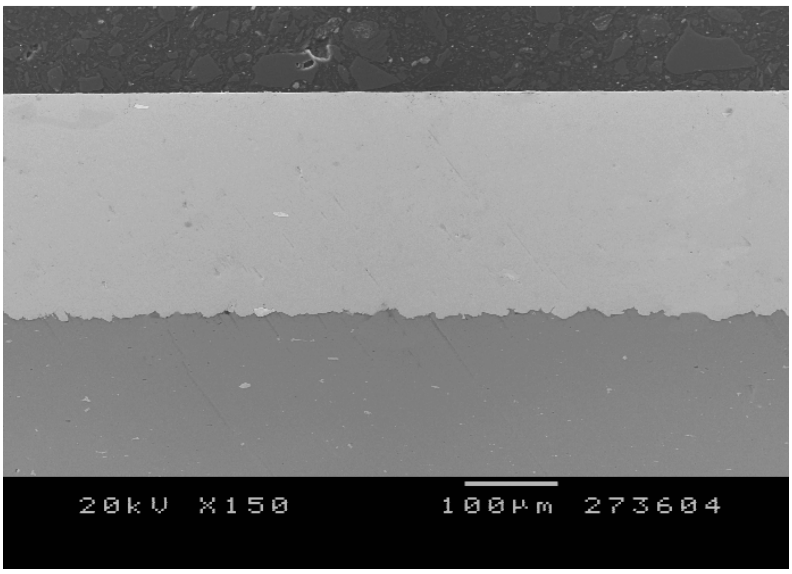

Figure 48 - Coating 12 after removing of the porous zone.

10. Conclusions

Since cold spray is a very recent technique, every new work in the subject allows the gathering of new and important information. This work is not an exception since it is the first written work about the deposition of pure titanium onto aluminium substrates.

Concerning the main objectives proposed at the beginning and in agreement with the experimental results following the factorial analysis, it can be concluded as following:

- Principally and most importantly, it was easily and fast obtained a dense pure titanium coating onto aluminium 7075, with thickness higher than 300μm and no microstructural changes, and also to better understand the bonding mechanisms.
- The effects of gas temperature, gas pressure, and powder feeding rate on cold sprayed pure titanium coatings onto aluminium substrates were investigated. All resulting coatings were characterized in terms of their microstructures, coating thickness and porosity and, micro-hardness. The best set of parameters was chosen and the corresponding coating was deeper characterized regarding its hardness profile, phase composition and particle distribution.
- The parameter that influences more the coating thickness, rising it, is the feeding rate. For the same feeding rate, the coating thickness increases with the temperature and decreases with the pressure. Coatings over 300μm thickness were easily achieved through cold spray.
- For titanium deposition, higher temperature results in a denser coating while high pressure increases the porosity due to an erosion effect provoked by the too high particle velocities.
- Mainly, temperature and pressure affect the plasticity of the particles: the higher the temperature is for the same pressure value, the more plastic will be the material and there will be less rebounding; on the other hand, for a same temperature, a higher pressure can be favourable for a better disposal of the particle to adhere to the substrate or a former bonded particle but, above a specific value, it can cause a ballistic effect leading to erosion, which in our case succeeded at 35-40bar.
- The particle size distribution is of greater importance in the cold spray process. A high size distribution leads to non-uniform coatings regarding thickness, porosity and hardness, and makes the process non-reliable since particles can either reach or not the critical velocity, and depending on the main fraction of the powder that composes the coating, the properties will vary a lot. When the distribution is

narrower, the process becomes reproducible, and the coating properties become more homogeneous.

- A powder with higher particle size, but narrow distribution, results in a thicker coating when compared with a powder of smaller particle size. However, the coating's properties are less uniform.
- Regarding the bond formation in cold spray, were found results that support either the occurrence of a solid-state diffusion with adiabatic shear instabilities. The bonding strength of the deposited coatings was around 34MPa with high potential to increase to 40MPa.
- After optimization, the cold spray process when compared to the conventional thermal spray techniques, results in coatings with very good properties and cost-time effective (higher coating thickness can be achieved in less time and with less money investment), making it ideal for industrial applications.
- When the external porous layer is mechanically removed, a fully dense coating is obtained.

11. Future Perspectives

Further mechanical and tribological tests are required in order to better characterize the titanium coating and its interaction with the substrate, mainly to which point it can protect it from corrosion. For this to be possible, it is proposed that the small porous zone of the coating is removed, giving origin to a completely uniform and virtually 100% dense coating, that should allow the application of the Al 7075 alloy in more aggressive environments. Also, more clarification is required about the bonding process, in particular the influence of the substrate preparation.

Regarding the future applications of the titanium coating onto aluminium substrates, a very important advantage would be the possible substitution of certain parts (those that the mechanical solicitation would allow for) of the airplanes that are made of expensive titanium alloys (Ti6Al4V for example), and other products of the transport industry like ships or green cars. This last approach would significantly decrease the cost and the fuel consumption, since it would replace an alloy of approximately 4.43 g/cm3 that costs 24000 US$/ton [49] for one of 2.81 g/cm3 that costs 1290 US$/ton [50].

Bibliography

[1] *aluMATTER* consulted on 27th April 2009 www.aluminium.matter.org.uk

[2] *ASM Metals Handbook Volume 2 - Properties and Selection: Nonferrous Alloys and Special-Purpose Materials*. ASM International 1992

[3] *Titanium - Properties, Advantages and Applications Solving The Corrosion Problems In Marine Service*. J. A. Mountford Jr. Paper number 02170 presented in Corrosion2002

[4] *Electrodeposition of Titanium on Base Metals*. M. E. Sibert, Journal of the Electrochemical Society, Volume 2, 105, 1955, pp. 641

[5] *Chemical Vapour Deposition: Precursors, Processes and Applications*. A.C. Jones et al. RSC Publishing, 2008, Chapter 1

[6] United States Patent 6294466 B1 of 25th September 2001

[7] *The cold spray materials deposition process: Fundamentals and applications*. V. K. Champagne, Woodhead Publishing in Materials, 2007

[8] *Handbook of Thermal Spray Technology*. C. C. Bernd et al., ASM International, 2004

[9] *No Vacuum Plasma* published in the Fraunhofer Magazine 1.2002, pp. 46-47

[10] Image obtained on the 22nd of April 2009 from http://www.plasmathermalcoatings.com/technologies.htm

[11] *Deposition efficiency, mechanical properties and coating roughness in cold-sprayed titanium*. R. S. Lima et al. Journal of Materials Science Letters, 21, 2002, pp. 1687-1687

[12] United Kingdom Patent nº 21006, 1911

[13] Image obtained on the 21st of April 2009 from http://www.sulzermetco.com/

[14] *The Science and Engineering of Thermal Spray Coatings*. L. Pawlowski, John Wiley & Sons, 1995

[15] *Standoff distance and bow shock phenomena in the Cold Spray process. J.* Pattison et al. Surface & Coatings Technology, 202, 2008, pp. 1443-1454

[16] *Critical particle velocity under cold spray conditions*. F. Raletz et al. Surface & Coatings Technology, 201, 2006, pp. 1942-1947

[17] *Cold Spray Deposition: Significance of Particle Impact Phenomena*. S. Klinkov et al. Aerospace Science and Technology, 10, 2005, vol. 9, no. 7, pp. 582-591.

[18] *Adiabatic shear instability based mechanism for particles/substrate bonding in the cold-gas dynamic-spray process*. M. Grujicic et al. Materials and Design, 25, 2004, pp. 681-688

[19] *Deposition characteristics of titanium coating in cold spraying*. C.-J. LI and W.-Y. Li, Surface and Coatings Technology, 167, 2003, pp. 278-293

[20] *Synthesis and mechanical properties of nanocrystalline Ni coatings produced by cold gas dynamic spraying*. L. Ajdelsztajn et al. Surface & Coatings Technology, 201, 2006, pp. 1166-1172

[21] *Kinetic spray coatings*. T. H. Van Steenkiste et al. Surface and Coatings Technology, 111, 1999, pp.62-71

[22] Image obtained on the 23rd of April 2009 from http://en.wikipedia.org/wiki/De_Laval_nozzle

[23] Cold *Spray Deposition of Nanocrystalline Aluminum Alloys*. L. Ajdelsztajn et al. Metallurgical and Materials Transactions A, 36A, March 2005, pp. 657

[24] *Synthesis and mechanical properties of nanocrystalline Ni coatings produced by cold gas dynamic spraying*. L. Ajdelsztajn et al. Surface & Coatings Technology, 201, 2006, pp. 1166-1172

[25] *Effect of the substrate surface activation on the process of cold spray coating formation*. A. N. Papyrin et al. ITSC 2005 "Thermal Spray connects: Explore its surfacing potential!" Basel, Switzerland, 2005, pp. 145-150

[26] *Development of a generalized parameter window for cold spray deposition. T.* Schmidt et al. *Acta Materialia,* 54, 2006, pp. 729-742

[27] *Effect of particle size, morphology, and hardness on cold gas dynamic sprayed aluminum alloy coatings*. B. Jodoin et al. Surface & Coatings Technology, 201, 2006, pp. 3422-3429

[28] *Cold gas dynamic spraying of a high temperature Al alloy. L.* Ajdelsztajn et al. Surface & Coatings Technology, 201, 2006, pp. 2109-2116

[29] *Particle loading effect in cold spray*. K. Taylor et al. ITSC 2005 "Thermal Spray connects: Explore its surfacing potential!" Basel, Switzerland, 2005, pp. 186-191

[30] LI, C.-J., et al. *Effect of Spray Angle on Deposition Characteristics in Cold Spraying*. ITSC 2003 "Advancing the Science & Applying the Technology", Ohio, USA, 2003, pp. 91-96

[31] *Analysis of cold gas dynamically sprayed aluminium deposits*. R. Morgan et al. Materials Letter, 58, 2004, pp. 1317-1320

[32] *Effect of particle geometry and substrate preparation in cold spray*. P. Richer et al. ITSC 2005 "Thermal Spray connects: Explore its surfacing potential!" Basel, Switzerland, *2005,* pp.193-1

[33] *Aluminium coatings via kinetic spray with relatively large powder particles*. T. H. Van Steenkiste et al. Surface and Coatings Technology, 154, 2002, pp. 237-252

[34] *Effect of Cold Spray Deposition of a Titanium Coating on Fatigue Behavior of a Titanium Alloy*. T. S. Price et al. Journal of Thermal Spray Technology, 15, 2006, pp. 507-512

[35] *Properties of SiC-Reinforced Aluminum Alloy Coatings Produced by the Cold Gas Dynamic Spraying Process. E.* Sansoucy et al. Surface & Coatings Technology, 2008, 202, p 3988-3996.

[36] *Gas Dynamic Principles of Cold Spray*. R. C. Dykhuizen et al. Journal of Thermal Spray Technology, 1998, 7(2), p. 205-212.

[37] *Bonding mechanism in cold gas spraying*. H. Assadi et al. Acta Materialia, 51, 2003, pp. 4379-4394

[38] *Dynamic amorphization and recrystallization of metals in kinetic spray process*. Y. Xiong et al. Applied Physics Letters, 92, 2008

[39] *Cold Gas Dynamic Spraying of Aluminium: The Role of Substrate Characteristics in Deposit Formation*. D. Zhang et al. Journal of Thermal Spray Technology, 14, 2005, pp. 109-116

[40] U. S. Army Research Laboratory consulted on 3rd of June 2009 http://www.arl.army.mil/www/default.cfm?Action=369&Page=375

[41] Potential Applications of Cold-Spray Technology in Automotive Manufacturing. R. C. McCune, ITSC 2003 "Advancing the Science & Applying the Technology", Ohio, USA, 2003, pp. 63-70

[42] Cold Spray Copper Application for Upper Stage Rocket Engine Design. J. Haynes et al. ITSC 2003 "Advancing the Science & Applying the Technology", Ohio, USA, 2003, pp. 79-83

[43] U. S. Patent 6129948, Oct. 10, 2000

[44] *Statistics for Analytical Chemistry*. J. C. Miller, 3rd ed, Ellis Horwood Limited 1993

[45] *Aluminum: Properties and Physical Metallurgy*. J. E. Hatch, ASM International, 1984

[46] Elimination of porosity in directly fabricated titanium via cold gas dynamic spraying. S. H. Zahiri et al. Journal of Materials Processing Technology, 209, 2009, pp. 922-929

[47] Grain refinement in a single titanium powder particle impacted at high velocity. K. Kim et al. Scripta Materiala, 51, 2008, pp. 768-771

[48] Unpublished results of the Thermal Spray Centre, University of Barcelona, 2009

[49] ADVFN – Free Stock Quotes consulted on 27th April 2009 http://www.advfn.com/quote_Titanium Metals_NYSE_TIE.html

[50] London Metal Exchange consulted on 27th April 2009 http://www.lme.co.uk/aluminiumalloy.asp

ANNEX 1 – Aluminium 7075-T6 basic properties

Physical Properties	Values	Comments
Density	2.81 g/cm3	AA; Typical

Mechanical Properties		Comments
Hardness, Brinell	150	AA; Typical; 500 g load; 10 mm ball
Hardness, Knoop	191	Converted from Brinell Hardness Value
Hardness, Rockwell A	53.5	Converted from Brinell Hardness Value
Hardness, Rockwell B	87	Converted from Brinell Hardness Value
Hardness, Vickers	175	Converted from Brinell Hardness Value
Ultimate Tensile Strength	572 MPa	AA; Typical
Tensile Yield Strength	503 MPa	AA; Typical
Elongation at Break	11.0 %	AA; Typical; 1/16 in. (1.6 mm) Thickness
	11.0 %	AA; Typical; 1/2 in. (12.7 mm) Diameter
Modulus of Elasticity	71.7 GPa	AA; Typical; Average of tension and compression. Compression modulus is about 2% greater than tensile modulus.
Poissons Ratio	0.330	
Fatigue Strength	159 MPa @# of Cycles 5.00e+8	completely reversed stress; RR Moore machine/specimen
Fracture Toughness	20.0 MPa-m½	K(IC) in S-L Direction
	25.0 MPa-m½	K(IC) in T-L Direction
	29.0 MPa-m½	K(IC) in L-T Direction
Machinability	70%	0-100 Scale of Aluminum Alloys
Shear Modulus	26.9 GPa	
Shear Strength	331 MPa	AA; Typical

Electrical Properties		Comments
Electrical Resistivity	0.00000515 ohm-cm	AA; Typical at 68Â°F

Thermal Properties		Comments
CTE, linear	23.6 µm/m-°C @Temperature 20.0 - 100 Â°C	AA; Typical; average over range
	25.2 µm/m-°C @Temperature 20.0 - 300 Â°C	average
Specific Heat Capacity	0.960 J/g-°C	
Thermal Conductivity	130 W/m-K	AA; Typical at 77Â°F
Melting Point	477 - 635.0 Â°C	AA; Typical range based on typical composition for wrought products 1/4 inch thickness or greater. Homogenization may raise eutectic melting temperature 20-40Â°F but usually does not eliminate eutectic melting.

Solidus	477 °C	AA; Typical
Liquidus	635.0 °C	AA; Typical

Processing Properties		Comments
Annealing Temperature	413 °C	
Solution Temperature	466 - 482 °C	
Aging Temperature	121 °C	

Composition		Comments
Aluminum, Al	87.1 - 91.4 %	As remainder
Chromium, Cr	0.18 - 0.280 %	
Copper, Cu	1.20 - 2.0 %	
Iron, Fe	<= 0.50 %	
Magnesium, Mg	2.10 - 2.90 %	
Manganese, Mn	<= 0.30 %	
Other, each	<= 0.050 %	
Other, total	<= 0.15 %	
Silicon, Si	<= 0.40 %	
Titanium, Ti	<= 0.20 %	
Zinc, Zn	5.10 - 6.10 %	

ANNEX 2 – Commercially pure grade 1 titanium basic properties

Physical Properties	Values	Comments
Density	4.51 g/cm3	

Mechanical Properties		Comments
Hardness, Brinell	120	annealed
Hardness, Knoop	132	Estimated from Brinell.
Hardness, Rockwell B	70	annealed
Hardness, Vickers	122	Estimated from Brinell.
Tensile Strength, Ultimate	240 MPa	
Tensile Strength, Yield	170 - 310 MPa	
Elongation at Break	24.0 %	
Reduction of Area	35.0 %	
Modulus of Elasticity	105 GPa	In Tension
Compressive Modulus	110 GPa	
Poissons Ratio	0.370	
Charpy Impact	310 J	V-notch
Shear Modulus	45.0 GPa	

Electrical Properties		Comments
Electrical Resistivity	0.0000450 ohm-cm	

Thermal Properties		Comments
Heat of Fusion	325 J/g	High Purity Ti.
CTE, linear	8.60 µm/m-°C @Temperature 0.000 - 100 Â°C 9.20 µm/m-°C @Temperature 0.000 - 315 Â°C	average
CTE, linear, Transverse to Flow	9.70 µm/m-°C @Temperature 0.000 - 540 Â°C	perpendicular to the c-axis
Specific Heat Capacity	0.520 J/g-°C	Heat Capacity at 540ºC is 0.67 J/g-ºC
Thermal Conductivity	16.0 W/m-K	annealed
Melting Point	<= 1670 °C	Liquidus
Liquidus	1670 °C	
Beta Transus	888 °C	

Optical Properties		Comments
Emissivity (0-1)	0.300	High purity Ti at 710°C

Reflection Coefficient, Visible (0-1)	0.560	High purity Ti; visible light.

Composition		Comments
Carbon, C	<= 0.10 %	
H	<= 0.015 %	
Iron, Fe	<= 0.20 %	
Nitrogen, N	<= 0.030 %	
Oxygen, O	<= 0.18 %	
Titanium, Ti	99.5 %	